

We are IntechOpen, the world's leading publisher of Open Access books Built by scientists, for scientists

6,300

Open access books available

171,000

International authors and editors

190M

Downloads

Our authors are among the

154

Countries delivered to

TOP 1%

most cited scientists

12.2%

Contributors from top 500 universities



WEB OF SCIENCE™

Selection of our books indexed in the Book Citation Index
in Web of Science™ Core Collection (BKCI)

Interested in publishing with us?
Contact book.department@intechopen.com

Numbers displayed above are based on latest data collected.
For more information visit www.intechopen.com



Effective Thermal Conductivity of Cupra and Polyester Fiber Assemblies in Low Fiber Volume Fraction

Morihiro Yoneda

Additional information is available at the end of the chapter

<http://dx.doi.org/10.5772/intechopen.75604>

Abstract

In this study, the effective thermal conductivity of staple fiber assembly for wadding use is measured using KES-F7 II Thermo Labo II apparatus. Sample used are cupra, polyester (with round and heteromorphic section), and polytrimethylene terephthalate (PTT) fibers. Heat flux to calculate thermal conductivity is measured including heat leakage from sidewall and is calibrated in the analysis. Results are analyzed by nonlinear regression method. Results are obtained as follows. Thermal conductivity curve is convex downward in low fiber volume fraction (<3%). Thermal conductivity, λ , is expressed as following equation, $\lambda = A\phi + B/\phi + C$, where ϕ is fiber volume fraction, A and B are coefficients, and C is constant determined by nonlinear regression analysis. Based on this equation, the effective thermal conductivity is divided into three parts: $A\phi$, heat conduction in fiber; B/ϕ , radiative heat transfer; and C, heat conduction within air. By calibration, C component is divided into thermal conductivity of air, λ_{air} and heat leakage from sidewall of the sample frame. λ_{air} plays the most important role in thermal insulation property of fiber assembly, and component of heat conduction in fiber, $A\phi$, follows in higher fiber volume fraction. Component of radiative heat transfer, B/ϕ , is negligible small.

Keywords: effective thermal conductivity, fiber assembly, cupra fiber, polyester fiber, nonlinear regression

1. Introduction

In this chapter, a method to evaluate thermal insulation properties of staple fiber assembly for wadding use is proposed. Fiber assembly in low fiber volume fraction is a system which consists of a lot of air and a small amount of fiber, and its heat transfer mechanism is supposed to include convective and radiative heat transfer in addition to conductive heat transfer.

Therefore, it is not suitable to use thermal conductivity to evaluate thermophysical properties of fiber assembly. Instead, a concept of effective thermal conductivity is suitable to evaluate thermophysical properties of fiber assembly which can include different types of heat transfer mechanisms such as conduction, convection, and radiation. In this chapter, the effective thermal conductivity is used to evaluate thermal insulation properties of fiber assembly in low Fiber volume fraction, Φ for wadding use. In addition, a model to explain heat transfer mechanism within fiber assembly is proposed.

Effective thermal conductivity is measured based on guarded hot plate (GHP) method using KES-F7II Thermo Labo II apparatus (Kato Tech Ltd.). Fiber sample is put uniformly into sample frame made of polystyrene foam. In the measurement, sample system made of fiber assembly and sample frame is placed between heat source plate and heat sink, and heat flow to keep heat source temperature constant is measured.

Samples used are polyethylene terephthalate and cupra staple fiber assembly. Effective thermal conductivity is measured under various sample thickness and fiber volume fraction. The results are analyzed based on nonlinear regression method, and heat transfer mechanism within fiber assembly is discussed based on the result of analysis. Finally, designing of fiber assembly-based thermal insulation materials is investigated.

2. Background

Studies on heat conduction of fiber assembly have been conducted by Nogai et al. [1, 2], Fujimoto et al. [3], and Ohmura et al. [4] in Japan. Nogai et al. carried out theoretical and experimental study of heat transfer mechanism of polyester fiber assembly [1, 2]. Fujimoto et al. investigated the effective thermal conductivity of clothing materials for protection against cold [3]. Ohmura et al. studied the effective thermal conductivity of fibrous thermal insulation materials for building [4].

In all papers, it is confirmed that effective thermal conductivity- fiber volume fraction curve in low fiber volume fraction (<10%) shows the shape of convex downward. The fact that effective thermal conductivity curve has a minimum value gives a reason that fiber assembly have been widely used for thermal insulation materials. The minimum value in effective thermal conductivity curve was explained by increasing radiative heat transfer through pore space with increasing porosity based on their experimental and theoretical results and heat transfer model. Nogai et al. [1, 2] derived these facts based on uniaxial-oriented fiber assembly model considering conduction in fiber and radiative heat transfer. Fujimoto et al. [3] derived these facts based on serial-parallel model of heat transfer which is composed of fiber and pore part including radiative heat transfer.

In this study, effective thermal conductivity of fiber assembly in low fiber volume fraction is analyzed using empirical equation by nonlinear regression method [4–7]. The reason that fiber assembly has been used for thermal insulation materials is further investigated through the separation of heat transfer component of effective thermal conductivity.

3. Method

3.1. Materials

Four kinds of fiber materials used in this experiment such as cupra fiber (CU), polyester fiber with round section (RPE), polyester fiber with heteromorphic (W-shape) section (WPE), and polytrimethylene terephthalate fiber (PTT) of which fineness and fiber length are almost the same. The web after opening and carding process is conditioned under the environment of 20°C and 65% RH for 24 h. Fiber assembly is served as sample after conditioning. The details of fiber samples are shown in **Table 1**.

Main parameter for the measurement of effective thermal conductivity is fiber volume fraction in this experiment. Thermophysical properties for different fiber materials which have different specific gravity are compared under the same fiber volume fraction. Fiber volume fraction is defined as the ratio of fiber volume to apparent volume of fiber assembly. Fiber volume fraction Φ is calculated using following equation.

$$\Phi = \frac{W}{\rho_f d h^2} \quad (1)$$

where W is sample weight (g), ρ_f is specific gravity of fiber (n.d.), h is side length of heat plate (cm), and d is thickness of sample (cm). Staple fiber sample (W g) is filled uniformly into the space surrounded by wall of polystyrene foam of which inner size is 5 cm square and constant height (2, 3, and 5 cm). **Figure 1** shows sample frame filled with fiber assembly. **Figure 2** shows a plan of sample frame.

In this experiment, the effect of fiber volume fraction and sample thickness on effective thermal conductivity of fiber assembly is investigated. Fiber volume fraction is changed by five

Sample code	Detail of sample	Fineness (dtex)	Fiber length (mm)	Fiber diameter (μm)	Specific gravity (n.d.)	Percentage of crimp (%)
CU	Cupra-ammonium (Cupra) staple fiber	1.4	38	11.84	1.50	8.79
RPE	Polyester staple fiber with round section	1.3	38	12.76	1.38	26.70
WPE	Polyester staple fiber with w-shaped heteromorphic section	1.4	38	24.22 ^{*1} 6.27 ^{*2}	1.38	14.80
PTT	Polytrimethyleneterephthalate staple fiber	1.7	51	15.02	1.34	15.43

*1: a longer axis, *2: a minor axis

Table 1. Details of fiber samples for wadding use.

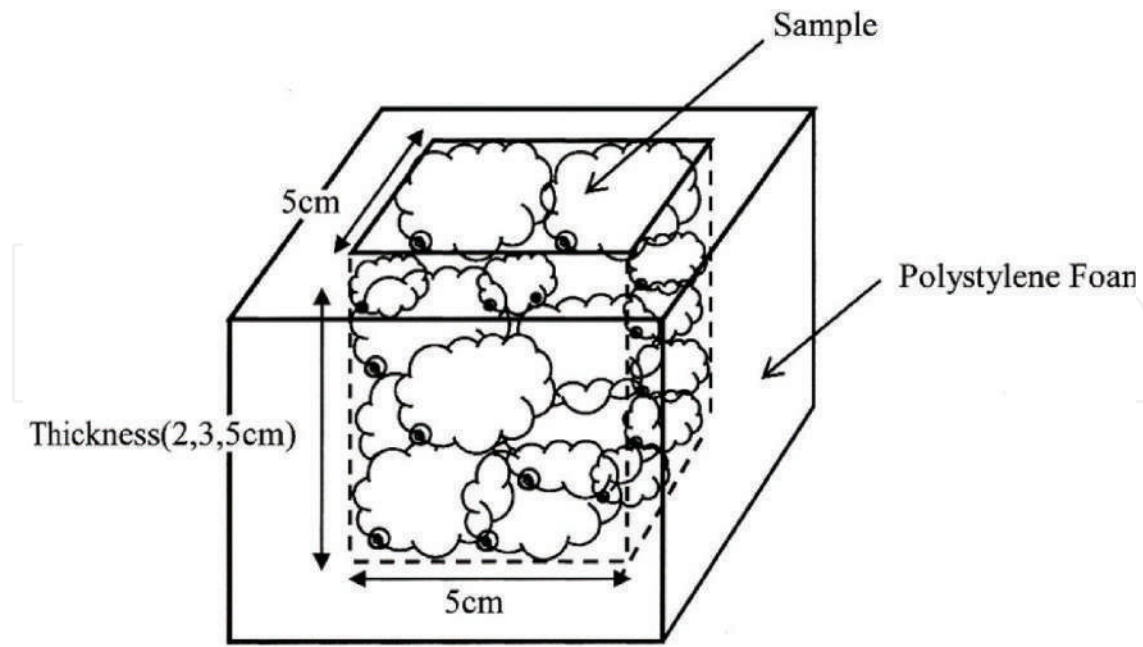


Figure 1. Schematic diagram of filling fiber sample into frame made of polystyrene foam.

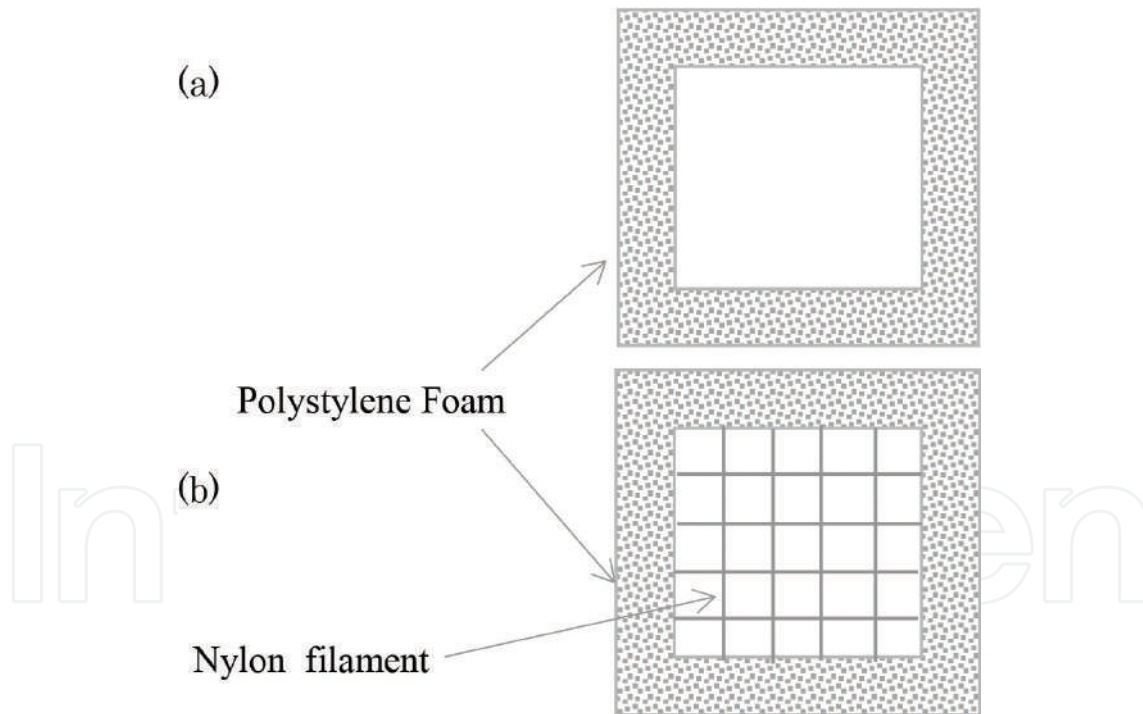


Figure 2. Frame made of polystyrene foam (a) top view and (b) bottom view.

stages such as 0.001, 0.005, 0.010, 0.025, and 0.030. Sample thickness is changed by three stages such as 2, 3, and 5 cm. One kind of fiber is, therefore, measured under 15 conditions. Sample weight for each fiber under different condition is shown in **Table 2**.

3.2. Measurement method

Effective thermal conductivity is measured using KES-F7II Thermo Labo II apparatus (Kato Tech Ltd.) [8]. Heat flux which flows through fabric sample from heat source plate (BT-Box) to heat sink is measured based on guarded hot plate (GHP) method. Schematic diagram of measurement part (section) is shown in **Figure 3**. Fiber sample is put uniformly into frame made of polystyrene foam of which inner size is 5 cm square and constant thickness. Fiber assembly with sample frame is placed between heat source plate and heat sink and measurement of heat flow is carried out. The experiment is conducted in a controlled environment room of which temperature is 20°C and humidity is 65% RH.

Heat source temperature (BT-Box) is set at 30°C and temperature of heat sink is set at 20°C, and thus, temperature difference is 10°C. Heat source plate is placed on upper side of sample and heat sink is placed on lower side, and thus the direction of heat flow agrees with the direction of acceleration of gravity. Upper side of heat sink is made of metal plate and temperature of heat sink is controlled at 20°C by cooling device driven by Peltier element.

Sample	Volume fraction	Thickness of a sample		
		2cm	3cm	5cm
Cupra	0.001	0.075	0.113	0.188
	0.005	0.375	0.563	0.938
	0.010	0.750	1.125	1.875
	0.025	1.875	2.813	4.688
	0.030	2.250	3.375	5.625
Polyester	0.001	0.069	0.104	0.173
	0.005	0.345	0.518	0.863
	0.010	0.690	1.035	1.725
	0.025	1.725	2.588	4.313
	0.030	2.070	3.105	5.175
PTT	0.001	0.067	0.101	0.168
	0.005	0.335	0.503	0.838
	0.010	0.670	1.005	1.675
	0.025	1.675	2.513	4.188
	0.030	2.010	3.015	5.025

Table 2. Sample weight for each measurement condition (unit: G).

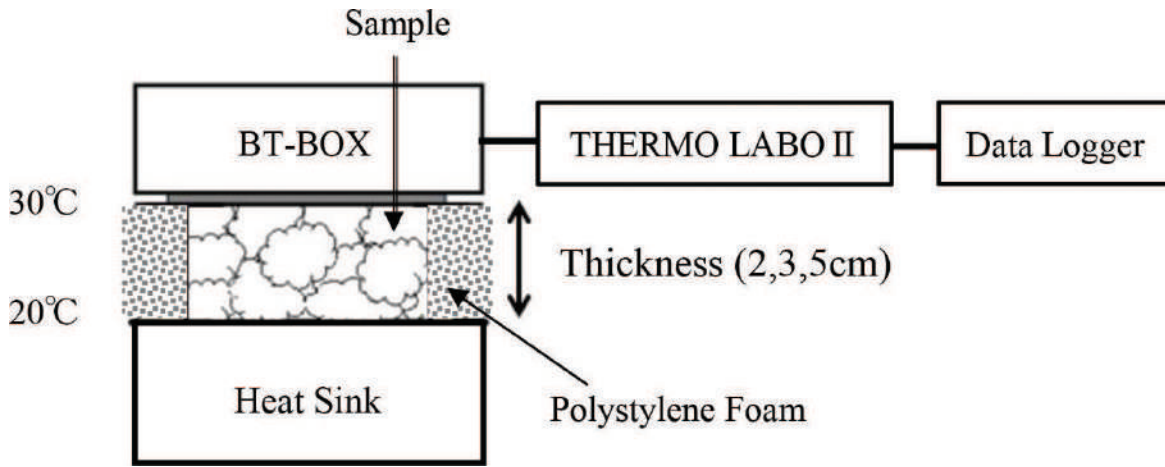


Figure 3. Measurement of thermal conductivity.

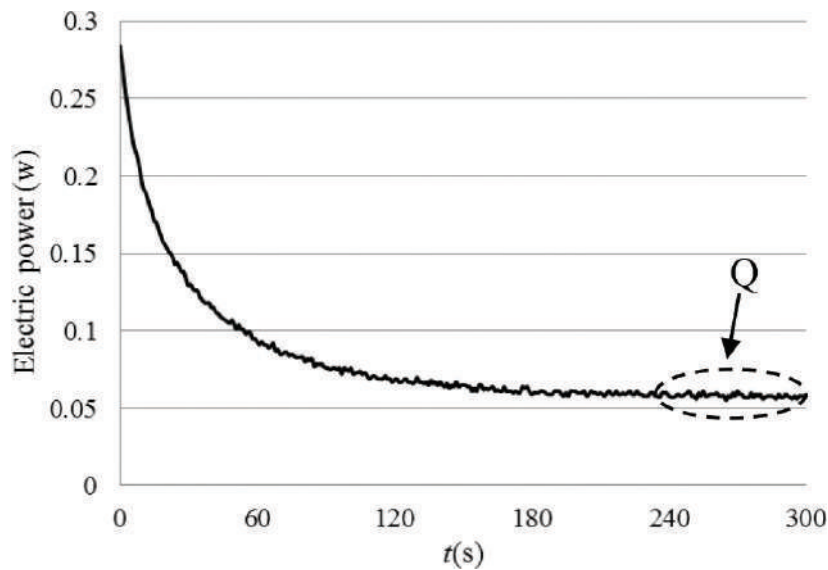


Figure 4. Method to obtain heat flux in steady state.

In the measurement, fiber assembly with sample frame is placed between heat source plate and heat sink, and electric power (W) is measured to keep heat source temperature steady state. Output signal of electric power is recorded with data logger which is connected to output terminal. Output signal is recorded at intervals of 1 s with time elapsed. An example of measurement is shown in **Figure 4**. Electric power is recorded against time from the contact between heat source and sample to the steady state. Electric power, Q (W), is obtained from mean value between 4 and 5 min. Effective thermal conductivity, λ (W/mK), is calculated from the following equation:

$$\lambda = \frac{Qd}{A\Delta T} \quad (2)$$

where Q is electric power to keep steady state (W), d is sample thickness (m), A is area of heat source plate, and ΔT is temperature difference between heat source plate and heat sink (K).

In this experiment, a small amount of heat flow through insulation material is measured. Therefore, care must be taken so that measurement part (BT-Box and heat sink) is not affected by unexpected influence of heat caused by convective and radiative heat transfer. As for radiative heat transfer, board made of polystyrene foam is set up in the front, right, and left side of measurement part to block radiative heat transfer from operator. As for convective heat transfer, it is desirable that a device which may cause convection should be removed from the place where experiment is conducted.

4. Results

Effective thermal conductivity of staple fiber assembly is measured under three different thickness and five different fiber volume fractions. Results obtained from the measurement are investigated in connection with fiber volume fraction, sample thickness, fiber materials, and so on. In this experiment, three times of measurement were carried out for each condition, and mean value and standard deviation were obtained.

In the first place, the relation between effective thermal conductivity and fiber volume fraction is investigated in relation to fiber material. **Figures 5–7** show the results between effective thermal conductivity and fiber volume fraction. **Figures 5–7** show the results of 2, 3, and 5 cm thickness, respectively. In each graph, the ordinate denotes effective thermal conductivity (W/mK) and the abscissa denotes fiber volume fraction (n.d.). The fact that the level of the magnitude of thermal conductivity increases with increasing thickness is observed and this will be discussed later. Here, we concentrate on the relation between effective thermal conductivity and fiber

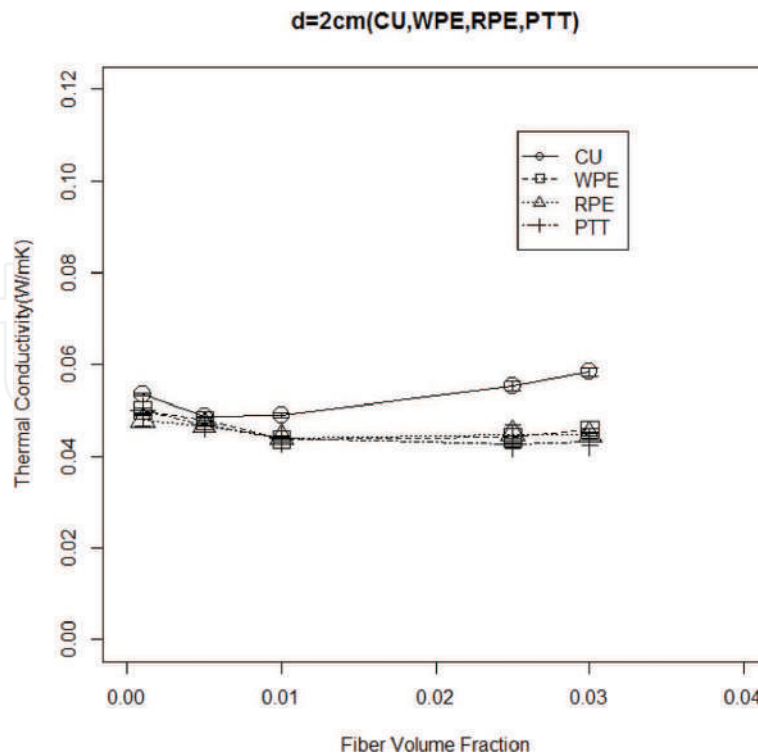


Figure 5. Thermal conductivity plotted against fiber volume fraction when thickness of sample is 2 cm.

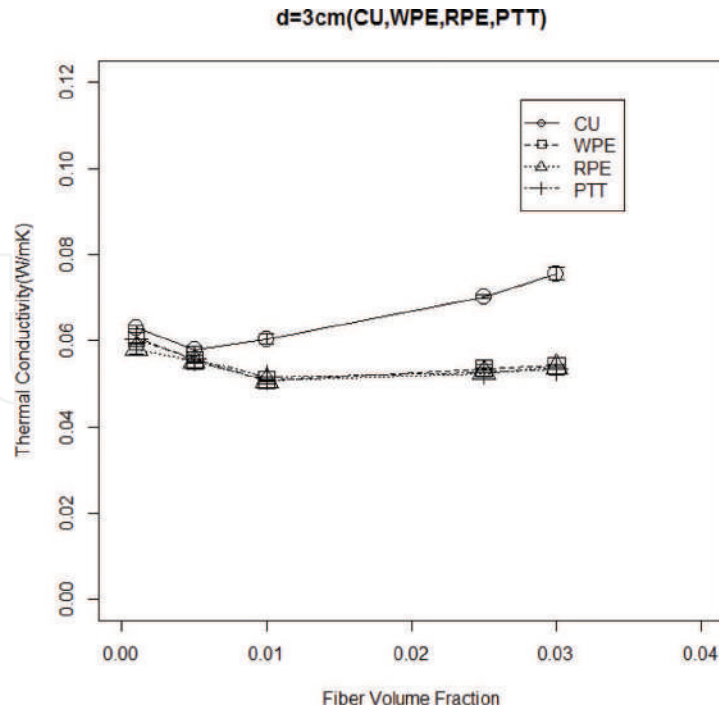


Figure 6. Thermal conductivity plotted against fiber volume fraction when thickness of sample is 3 cm.

volume fraction for the result of 5-cm thickness. Magnitude of effective thermal conductivity is compared under constant thickness. CU is the largest and polyester fiber group (RPE, WPE, PTT) follows. There is no significant difference among RPE, WPE, and PTT within the range of this method.

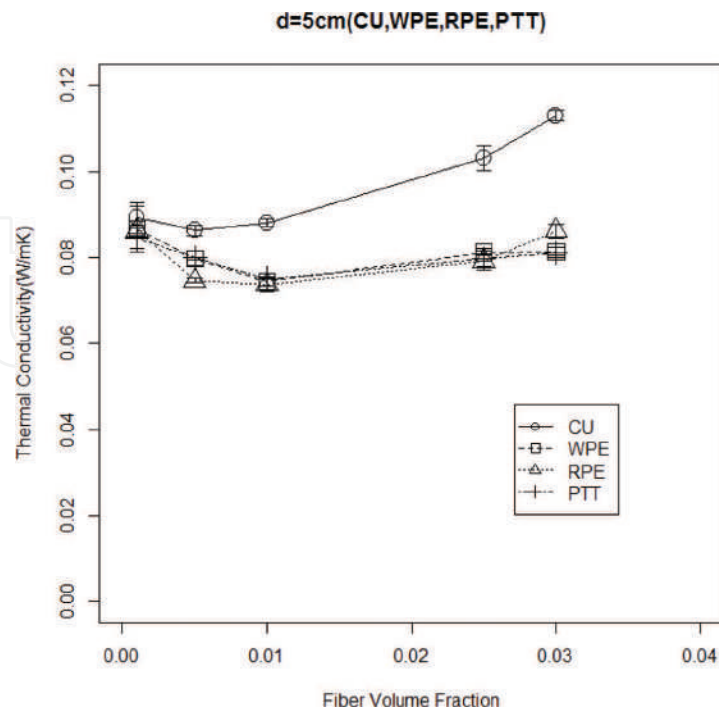


Figure 7. Thermal conductivity plotted against fiber volume fraction when thickness of sample is 5 cm.

Next, the effect of fiber material on the relation between effective thermal conductivity and fiber volume fraction is investigated. For each material, the shape of thermal conductivity curve is convex downward. The feature of the curve for each fiber material is as follows.

For CU, the minimum value of thermal conductivity lies around $\phi = 0.005$ and thermal conductivity increases with increasing ϕ . For RPE, WPE, and PTT, the minimum value of thermal conductivity lies around $\phi = 0.01$ and thermal conductivity increases a little to $\phi = 0.03$. For CU, thermal conductivity increases a little when ϕ decreases from 0.005 to 0.001. For RPE, WPE, and PTT, thermal conductivity increases a little when ϕ decreases from 0.01 to 0.001. With decreasing thickness from 3 to 2 cm, the level of thermal conductivity decreases and the shape of curve becomes flattened.

Figure 8 shows the relationship between effective thermal conductivity and sample thickness for $\phi = 0.01$. The ordinate denotes effective thermal conductivity and the abscissa denotes sample thickness. Clearly, thermal conductivity increases linearly against thickness for all samples.

Effective thermal conductivity obtained in this section is tentative value including leakage of heat from sidewall. In the following section, the separation of effective thermal conductivity into elemental process of heat transfer will be discussed. The thickness dependence of effective thermal conductivity shown in **Figure 8** will be investigated after the discussion about the separation heat transfer component.

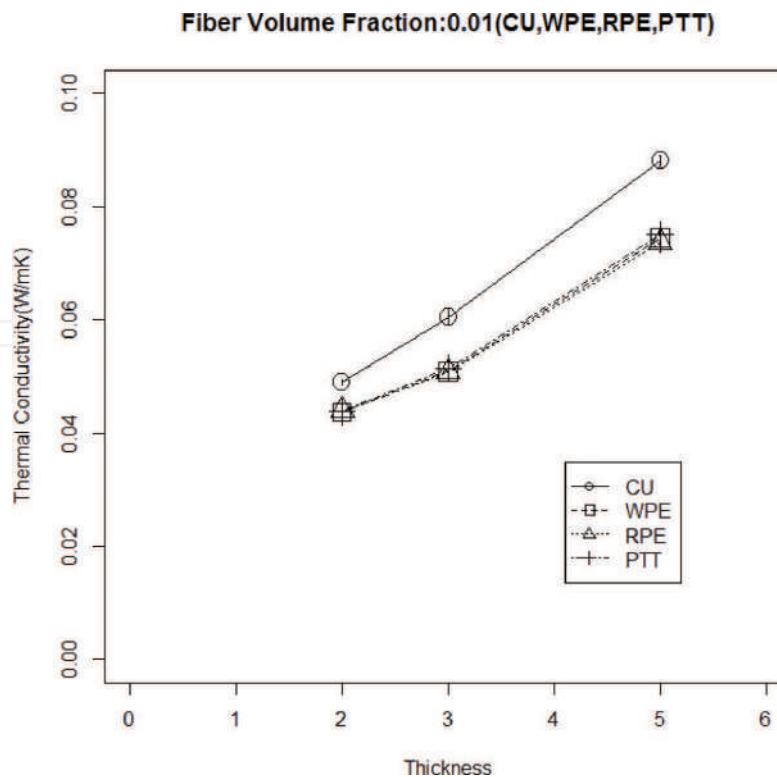


Figure 8. Thermal conductivity plotted against thickness when volume fraction of sample is 0.01.

5. Analysis

5.1. Analysis by nonlinear regression model

Because porosity of fiber assembly in this study is very large (97–99%), it is conjectured that the mechanism of heat transfer within fiber assembly is very much influenced by the effect originated from pore structure. The mechanism of heat transfer in fiber assembly consists of conduction in fiber, radiation in pore between fibers, and gas conduction (air), when forced convection does not occur. Here, it is supposed that heat flows through parallel model which is made of three components of heat transfer mentioned above. Measured value of effective thermal conductivity, λ (W/mK), is expressed by the following equation as a function of bulk density ρ (kg/m³) [4–7]:

$$\lambda = A\rho + B/\rho + C. \quad (3)$$

where A (Wm²/Kkg) and B (Wkg/m⁴K) are constant coefficients and C (W/mK) is constant. The first term at the right side denotes conductive heat transfer in fiber, the second term

Parameter	Sample code	Thickness of a sample		
		2cm	3cm	5cm
A	CU	4.51×10^{-1}	7.51×10^{-1}	1.04
	RPE	-2.45×10^{-2}	3.76×10^{-1}	5.54×10^{-1}
	WPE	-1.68×10^{-2}	7.68×10^{-2}	2.51×10^{-1}
	PTT	-1.04×10^{-1}	5.25×10^{-3}	1.83×10^{-1}
B	CU	9.03×10^{-6}	1.04×10^{-5}	1.05×10^{-5}
	RPE	2.73×10^{-6}	6.42×10^{-6}	1.89×10^{-5}
	WPE	5.20×10^{-6}	9.62×10^{-6}	1.30×10^{-5}
	PTT	4.68×10^{-6}	8.10×10^{-6}	9.75×10^{-6}
C	CU	4.41×10^{-2}	5.20×10^{-2}	7.78×10^{-2}
	RPE	4.52×10^{-2}	5.18×10^{-2}	6.70×10^{-2}
	WPE	4.51×10^{-2}	5.13×10^{-2}	7.36×10^{-2}
	PTT	4.54×10^{-2}	5.25×10^{-2}	7.48×10^{-2}
Air		2.62×10^{-2}	2.62×10^{-2}	2.62×10^{-2}

Table 3. List of coefficients A, B, and constant C.

denotes radiative heat transfer, and the third term denotes conductive heat transfer through gas (air) in pore. (The details of parameters A, B, and C are shown in the Appendix.)

In this study, bulk density, ρ in Eq. (3) is replaced by fiber volume fraction, ϕ as follows,

$$\lambda = A\phi + B/\phi + C. \quad (4)$$

This is because ϕ plays an equivalent role of ρ which expresses quantity of fiber. Results of the effective thermal conductivity of fiber assembly are analyzed by nonlinear regression method based on Eq. (4). Nonlinear regression analysis is carried out using **R** (ver. 3.1.1).

Estimated values of parameters A, B, and C obtained by nonlinear regression analysis are shown in **Table 3**, where A is coefficient of conduction in fiber, B is coefficient of radiative heat transfer, and C is conductive heat transfer in gas (constant). Calculated values of effective thermal conductivity using estimated values of A, B, and C are shown in **Figures 9–12**. **Figures 9–12** show the results of thickness of 2, 3, and 5 cm for CU, RPE, WPE, and PTT fiber, respectively. In each graph, the ordinate denotes effective thermal conductivity, λ (W/mK),

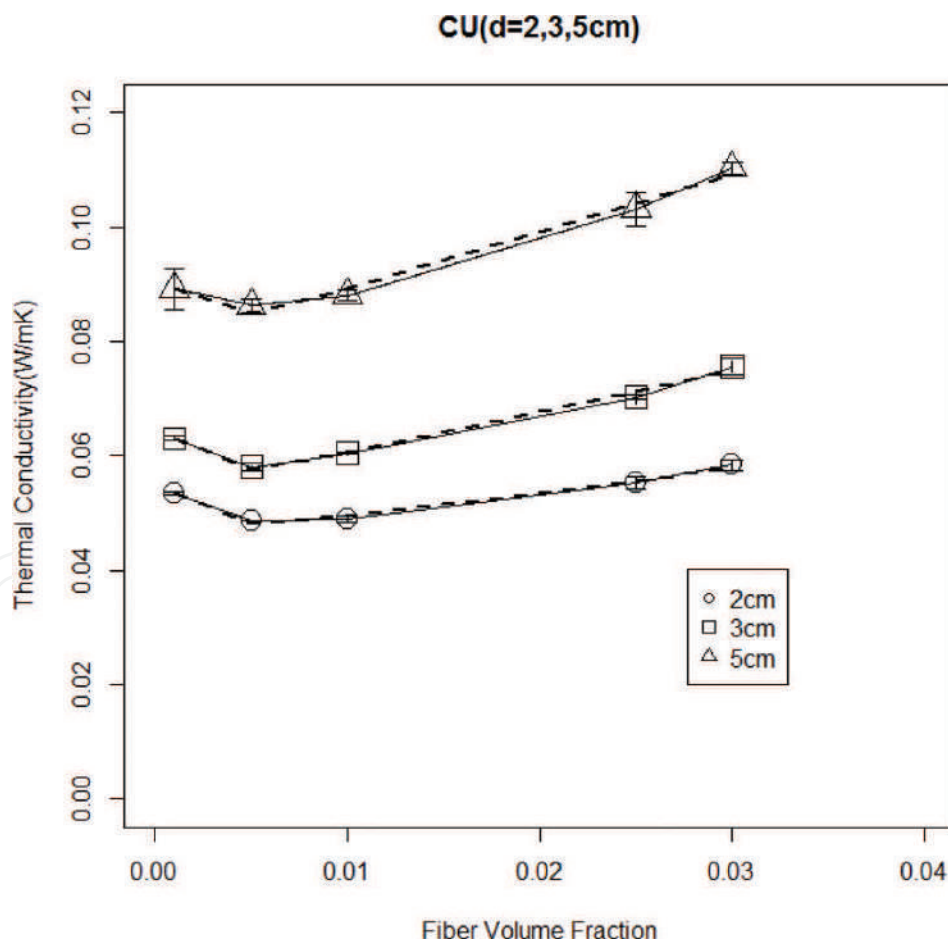


Figure 9. Comparison between calculated and measured values for CU. Symbols \circ , \square , Δ , and straight line: Measured values; broken line: Calculated values obtained by nonlinear regression analysis.

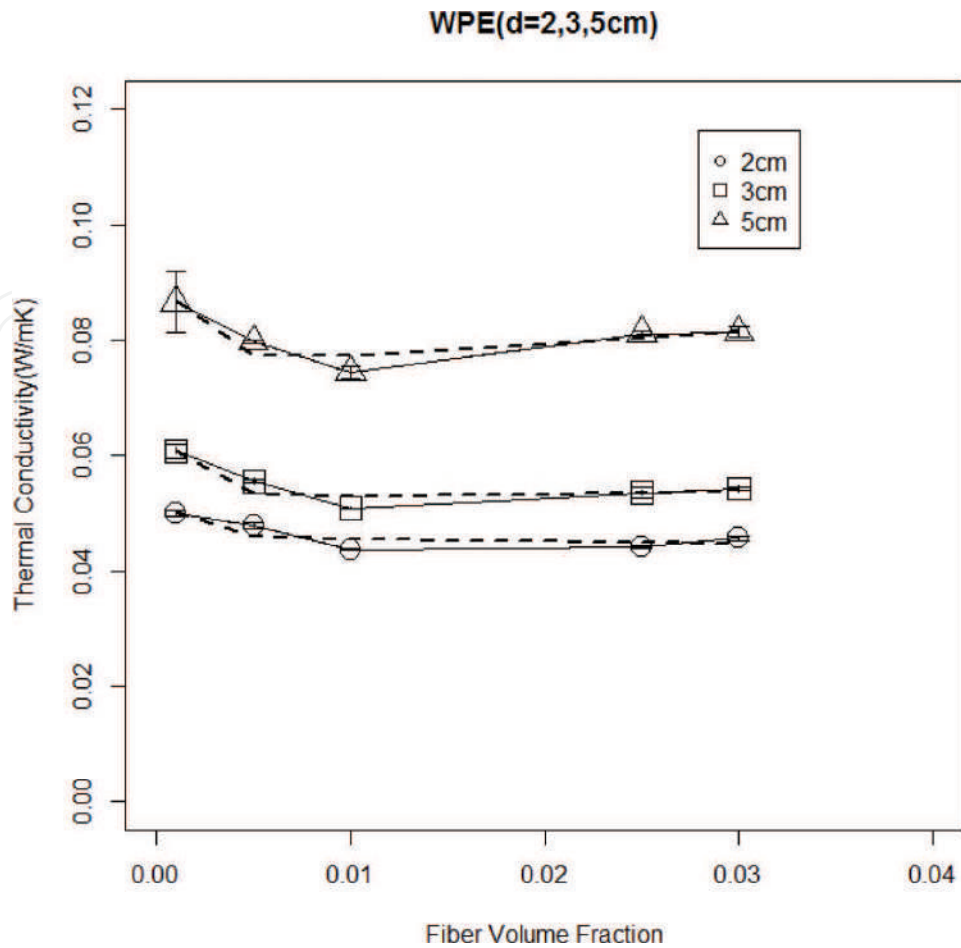


Figure 10. Comparison between calculated and measured values for WPE. Symbols \circ , \square , Δ , and straight line: Measured values; broken line: Calculated values obtained by nonlinear regression analysis.

and the abscissa denotes fiber volume fraction (n.d.). Symbols (\circ , Δ , \square) and solid line show measured values, and broken line shows regression curve using estimated values of A , B , and C . As shown in figures, agreement between measured and calculated curves of effective thermal conductivity is very good.

5.2. Analysis of heat transfer components

Calculated curves of separation of components using estimated values of A , B , and C are shown in **Figures 13–16**. **Figures 13–16** show the results of 3-cm thickness for CU, RPE, WPE, and PTT fiber, respectively. The ordinate denotes effective thermal conductivity, λ (W/mK), and the abscissa denotes fiber volume fraction, ϕ (n.d.). Dashed line shows component of conduction in fiber, $A\phi$, dash-dotted line shows component of radiative heat transfer, B/ϕ , two-dot chain line shows component of gas conduction, C , and solid line shows the measured value of effective thermal conductivity. Based on these graphs, the ratio of each component to effective thermal conductivity and the effect of pore in fiber assembly can be discussed for each fiber materials. It is clear that the ratio among $A\phi$, B/ϕ , and C is different for different fiber materials.

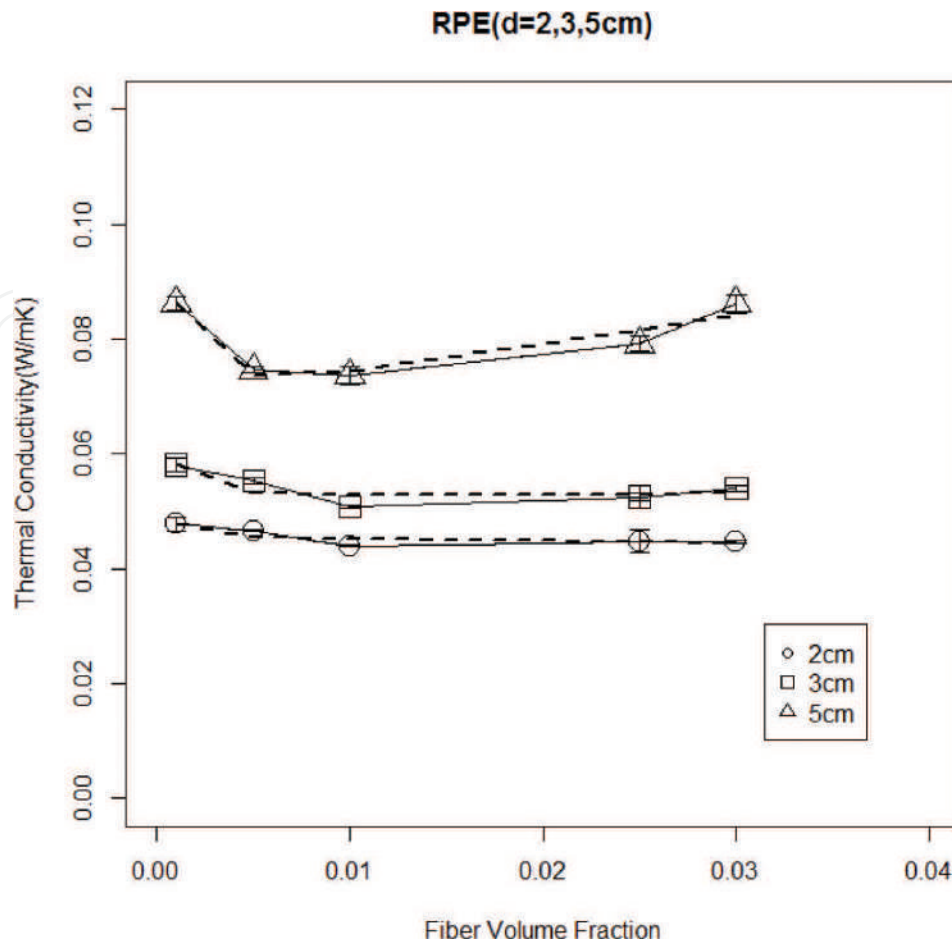


Figure 11. Comparison between calculated and measured values for RPE. Symbols \circ , \square , Δ , and straight line: Measured values; broken line: Calculated values obtained by nonlinear regression analysis.

First, component of conduction in fiber, $A\phi$ is investigated. Physical meaning of A is increasing rate of conduction in fiber against ϕ . As shown in **Table 3**, coefficient A varies with fiber materials. CU has large A value compared to polyester fibers (RPE, WPE, PTT), and increasing rate of conduction in fiber is also large. As a result, the ratio of $A\phi$ to effective thermal conductivity of CU is 30 percent at $\phi = 0.03$. In contrast, the ratio of $A\phi$ of WPE is less than 20% at $\phi = 0.03$. Large ratio of conduction in fiber and large increasing ratio to ϕ is the feature of CU fiber compared to polyester fibers.

Second, component of radiative heat transfer, B/ϕ , is investigated. Generally, the ratio of B/ϕ to effective thermal conductivity is negligibly small for all samples. Contribution of B/ϕ is slightly recognized below $\phi = 0.005$. It is observed that component of radiative heat transfer increases with decreasing fiber volume fraction, ϕ , from 0.005 to 0.001. In this study, the ratio of radiative heat transfer is very small compared to the previous results obtained by Nogai and Fujimoto [1–3]. This may arise from the difference in the degree of fiber orientation in fiber assembly. While Nogai and Fujimoto [1–3] cover fiber assembly with high degree of fiber orientation, we concentrate on fiber assembly with random orientation. Because frequency of collision between radiant heat and fiber is very large for randomly oriented fiber assembly, decay of radiation energy by absorption may become large.

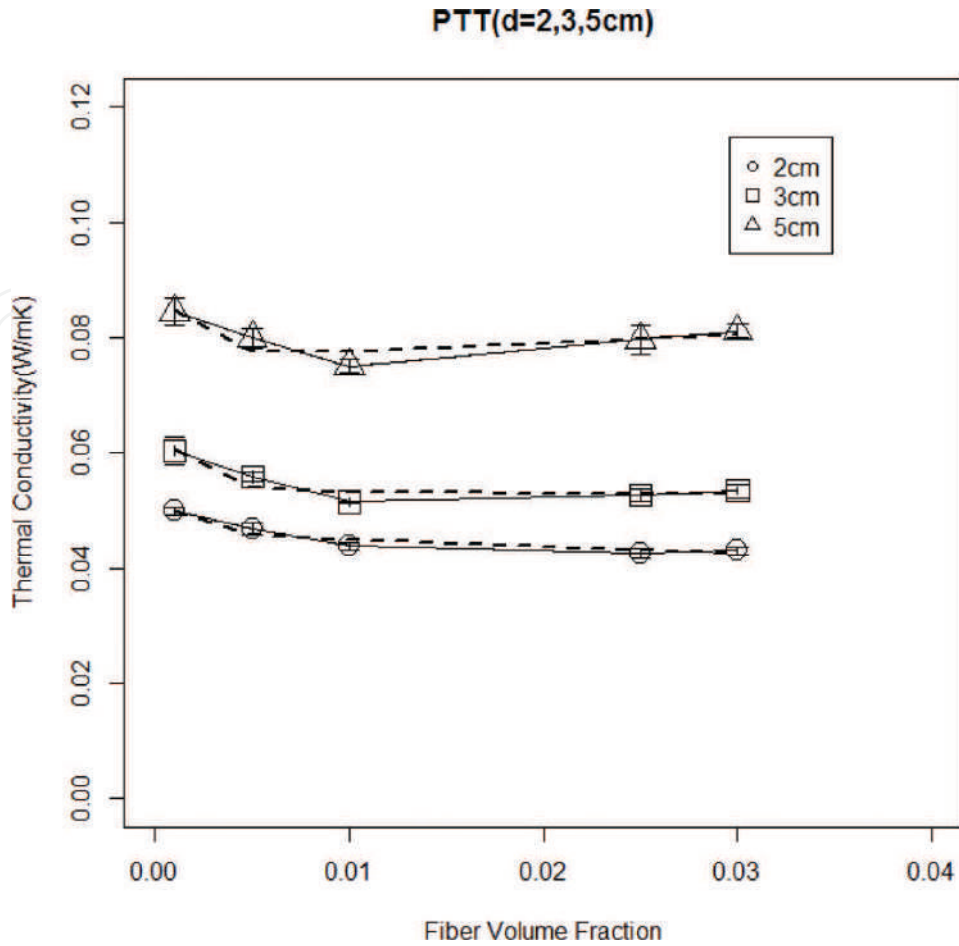


Figure 12. Comparison between calculated and measured values for PTT. Symbols \circ , \square , Δ , and straight line: Measured values; broken line: Calculated values obtained by using nonlinear regression analysis method.

5.3. Analysis of gas conduction

In this section, component of gas conduction, C , is investigated. Looking over **Figures 13–16**, it seems that component of gas conduction, C , occupies the dominant part in effective thermal conductivity in many cases. Therefore, physical meaning of gas conduction C is discussed, hereafter. Estimated values of C for samples of 2-, 3-, and 5-cm thickness are shown in the lower part of **Table 3**. It seems that C values for each thickness have almost constant value despite different samples. On the other hand, the value of thermal conductivity of air, λ_{air} , in this measurement condition (25°C, 1 atm) is 2.62×10^{-4} (W/mK) in Ref. [9]. Taking into consideration that parameter C has same value for same thickness and C must include thermal conductivity of air, λ_{air} , let us suppose that following relation holds:

$$C = \lambda_{\text{air}} + C' \quad (5)$$

where C' is constant independent of fiber volume fraction, ϕ . Mean values of each thickness, C_{mean} , thermal conductivity of air, λ_{air} and C' are shown in **Table 4** for the discussion in this section. It seems that C' increases with increasing thickness. Relation between C' and thickness

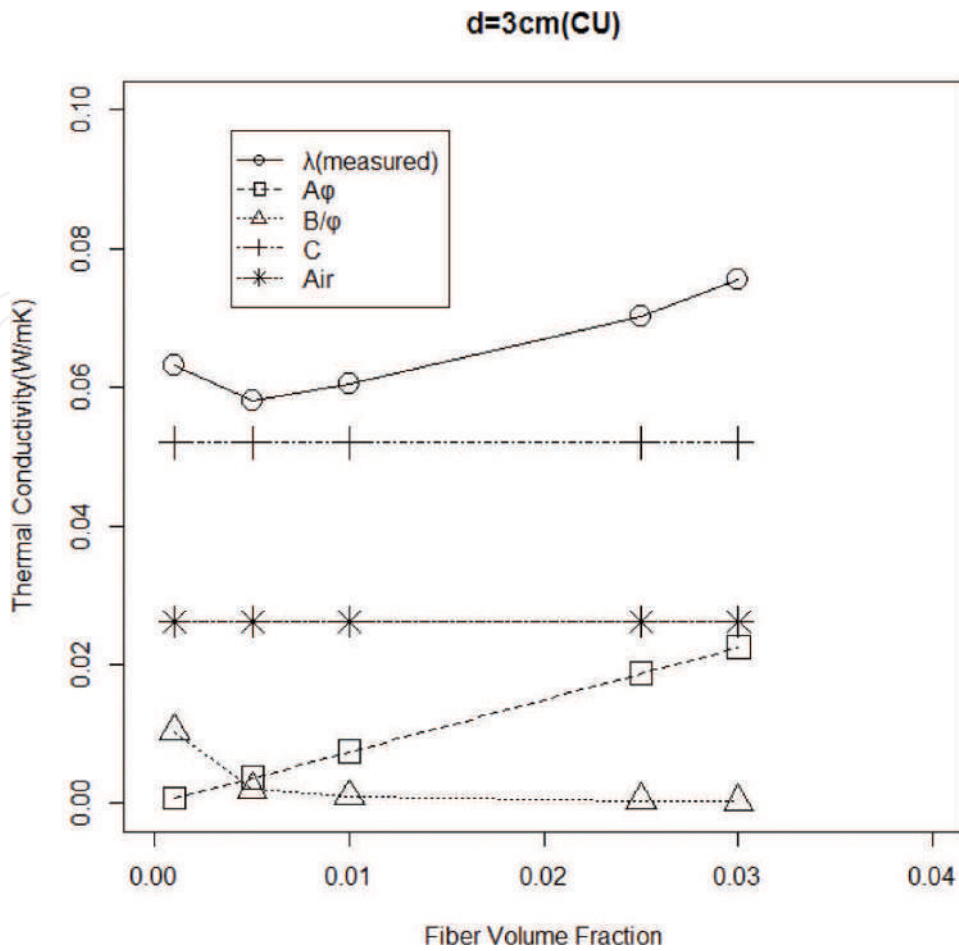


Figure 13. Separation of heat transfer component by nonlinear regression analysis for CU.

is analyzed by linear regression method. The results are shown in Figure 17. C' and thickness, d , have good correlation, and the regression equation is given as follows,

$$C' = 0.9325 d - 0.0425 \quad (R^2 = 0.996). \quad (6)$$

Because intercept is almost 0, C' can be expressed approximately as linear function of d :

$$C' = k d \quad (k:\text{constant}) \quad (7)$$

On the other hand, a function which expresses leakage of heat from sidewall of the frame is derived from another point of view. As inner side length of sample frame is 5 cm, total area of sidewall, A is expressed as following equation:

$$A = 4 \times 5 \times d \quad (\text{cm}^2). \quad (8)$$

Here, temperature gradient along thickness direction is ignored for the simplification. Thus, leakage of heat per unit area along horizontal direction is assumed to be constant. Total leakage of heat from sidewall, Q' , is proportional to total area of sidewall which is expressed as follows:

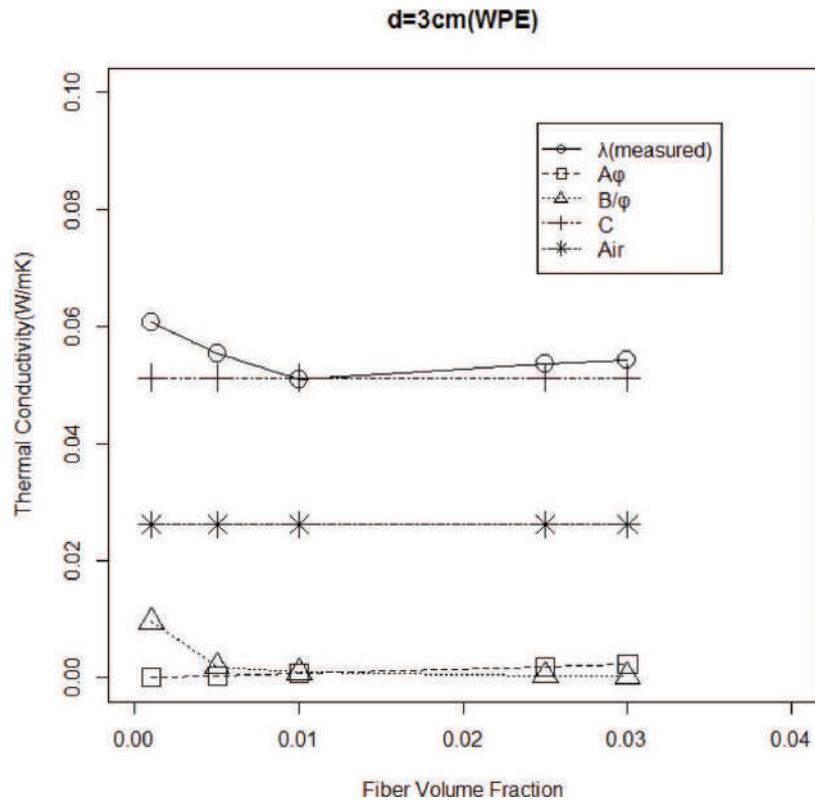


Figure 14. Separation of heat transfer component by nonlinear regression analysis for WPE.

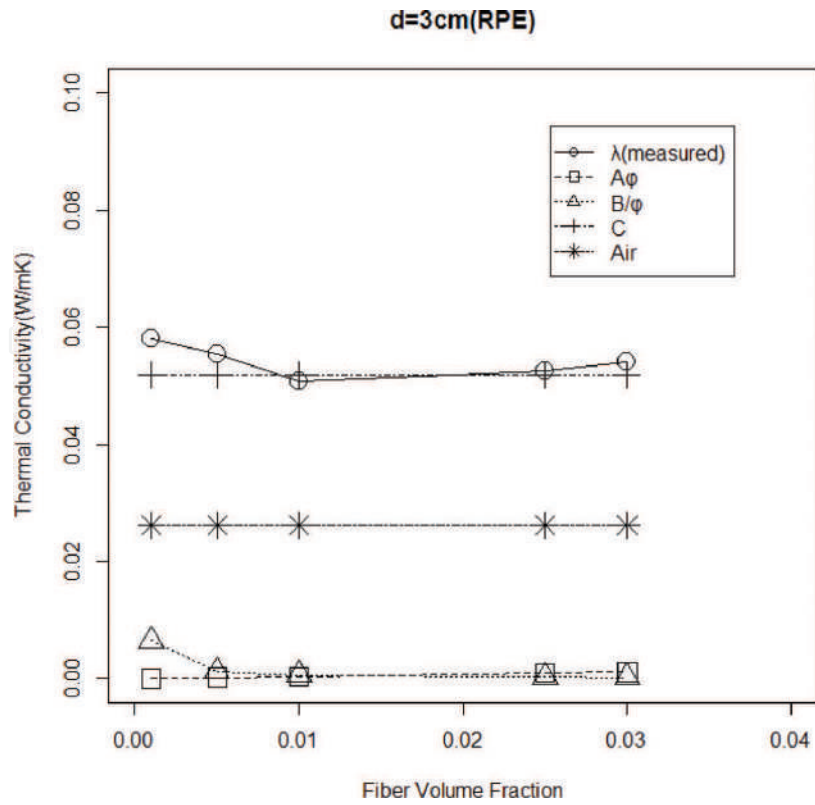


Figure 15. Separation of heat transfer component by nonlinear regression analysis for RPE.

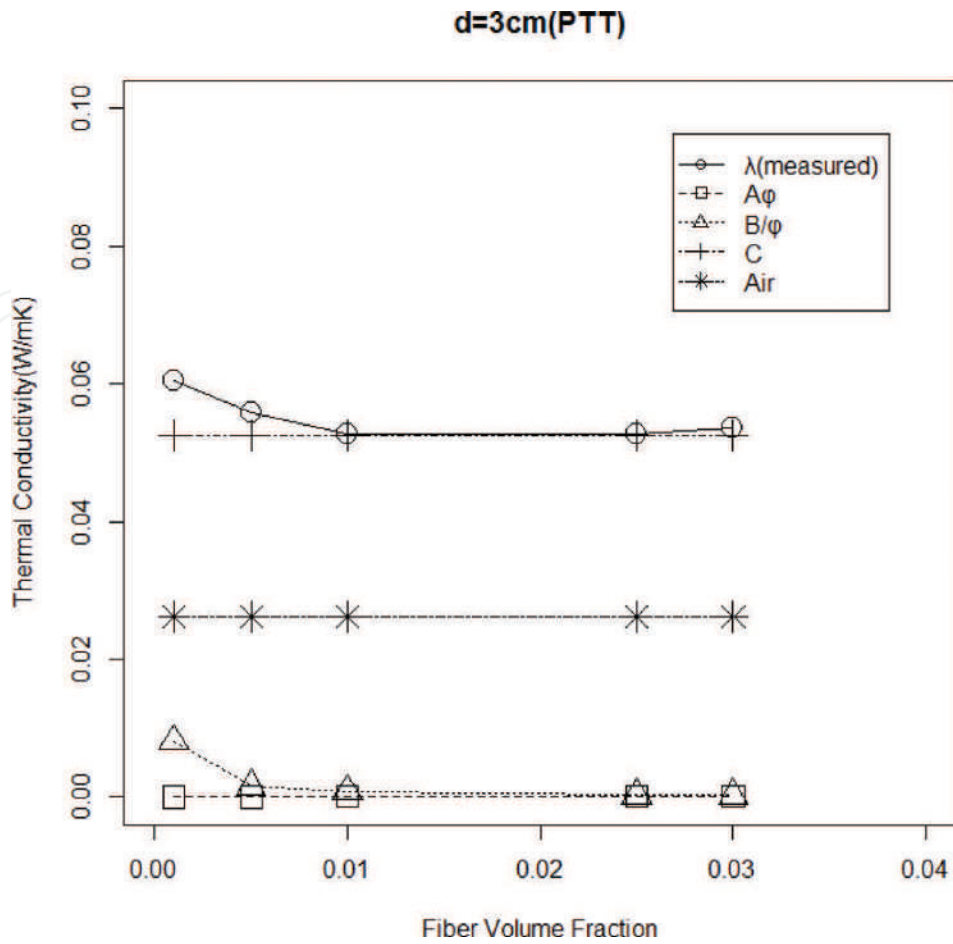


Figure 16. Separation of heat transfer component by nonlinear regression analysis for PTT.

$$Q' \propto A \propto d \tag{9}$$

This equation predicts that total leakage of heat from sidewall is proportional to thickness, d , and equals 0 at $d = 0$. This property coincides with the expression, $C' = k d$ in Eq. (7). Summarizing the discussion above, C' can be regarded as total leakage of heat from sidewall.

Based on the discussion above, total leakage of heat, C' , can be eliminated from C value. Here, C values in Figures 13–16 can be replaced by $\lambda_{\text{air}} (=C-C')$. The results are shown in Figures 18–21, where the abscissa denotes true effective thermal conductivity. It is concluded that large part

Thickness (cm)	C_{mean}	λ_{air}	C'
2	4.495×10^{-2}	2.62×10^{-2}	1.875×10^{-2}
3	5.19×10^{-2}	2.62×10^{-2}	2.57×10^{-2}
5	7.33×10^{-2}	2.62×10^{-2}	4.71×10^{-2}

Unit: W/mK

Table 4. Figures for calibration of leakage of heat.

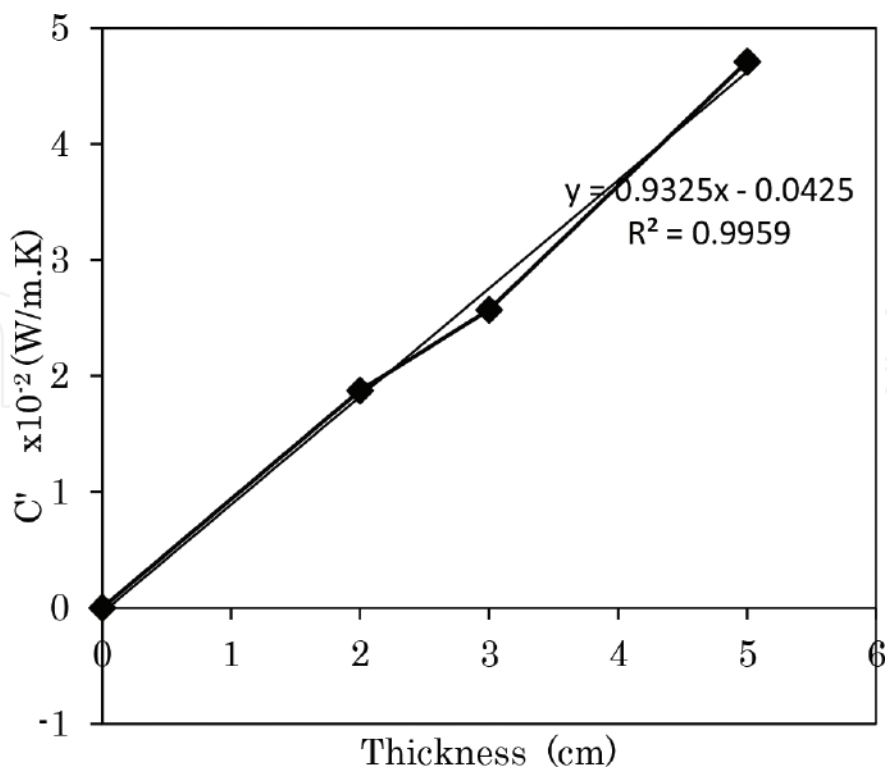


Figure 17. Function for the calibration of leakage of heat.

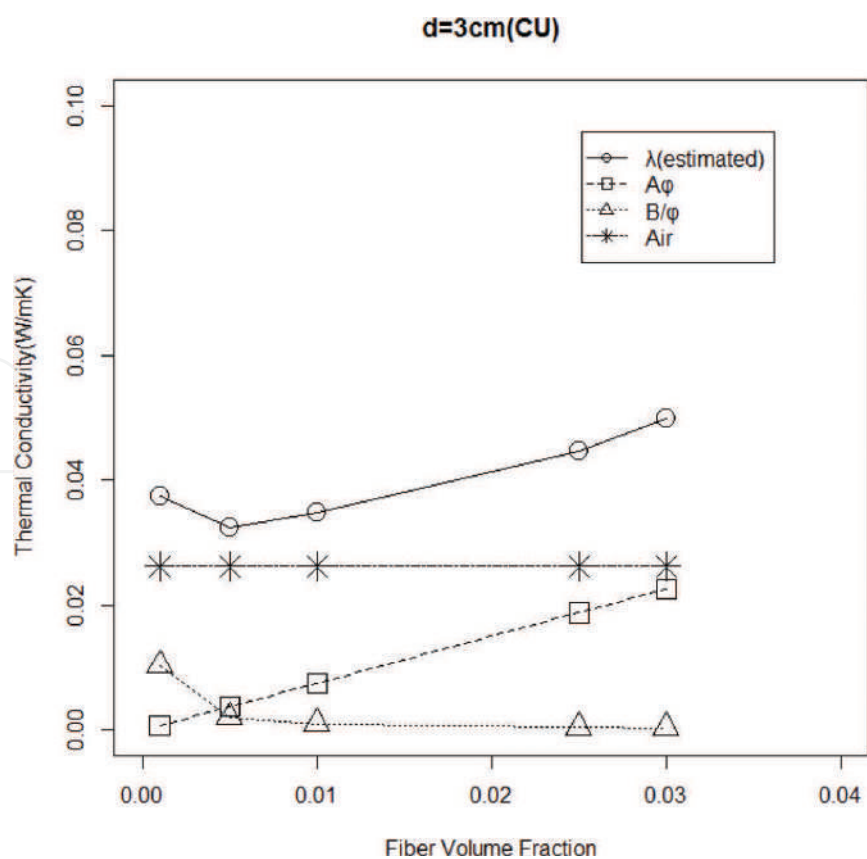


Figure 18. Estimated values of effective thermal conductivity and its component (sample: CU, d = 3 cm).

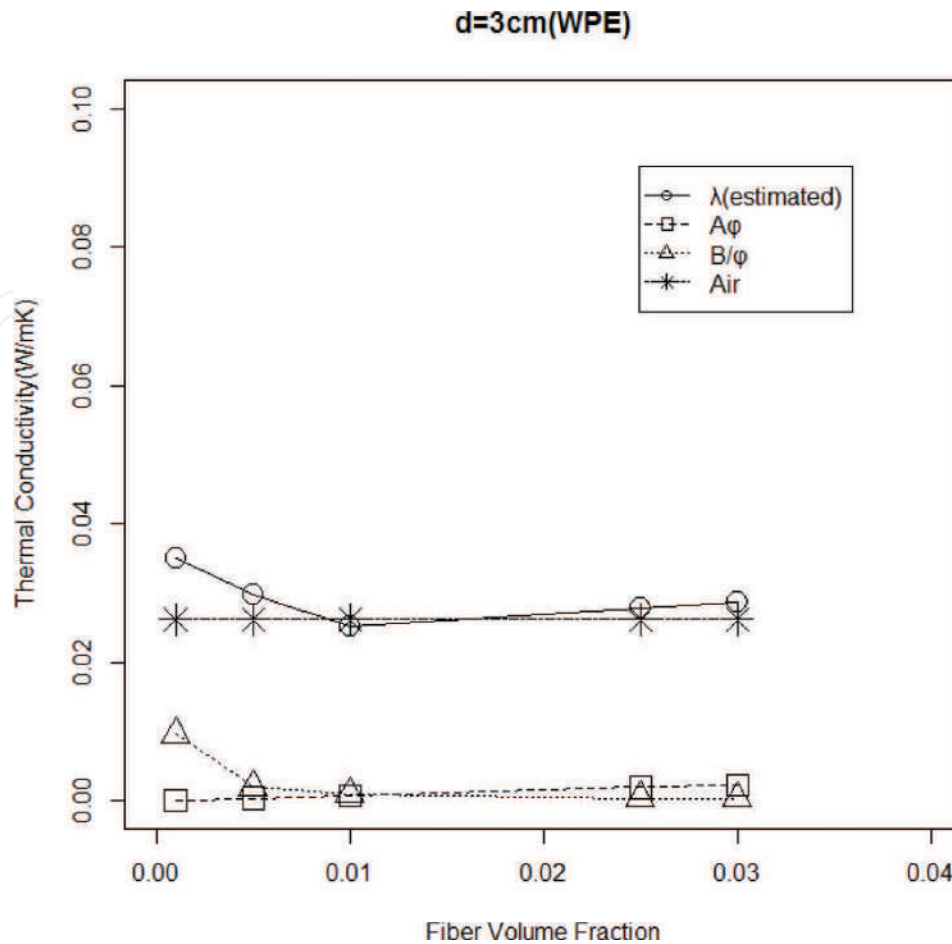


Figure 19. Estimated values of effective thermal conductivity and its component (sample: WPE, $d = 3$ cm).

of effective thermal conductivity of fiber assembly consists of thermal conductivity of air (still air), λ_{air} . It should be noted that the air is trapped by small amount of fiber ($\phi < 0.03$). (Explanation of this effect is given in the Appendix.)

Contribution of fiber material to the effective thermal conductivity is expressed by A , coefficient of conduction in fiber. Physical meaning of A is increasing rate of conduction in fiber and it consists of two parts, that is, heat conduction through fiber and heat conduction at contact point between fibers. It is conjectured that magnitude of A depends on contact effect between fibers compared to conduction through fiber. In this measurement, $A\phi$ component of cupra fiber (CU) is relatively large and that of polyester fibers (RPE, WPE, PTT) is relatively small. Polyester fibers have advantage in thermal insulation material because $A\phi$ component is small over the wide range of fiber volume fraction.

Based on nonlinear regression model, measured value of effective thermal conductivity can be separated into three components, such as conduction in fiber, radiative heat transfer, and gas conduction. Schematic diagram of the model is shown in Figure 22. Gas conduction plays the most important role in thermal insulation properties, which originates from immovable air trapped by fibrous network. Component of conduction in fiber has secondary contribution to thermal insulation properties, especially in the range of higher fiber volume fraction. Although radiative heat transfer slightly appears in low range of fiber volume fraction,

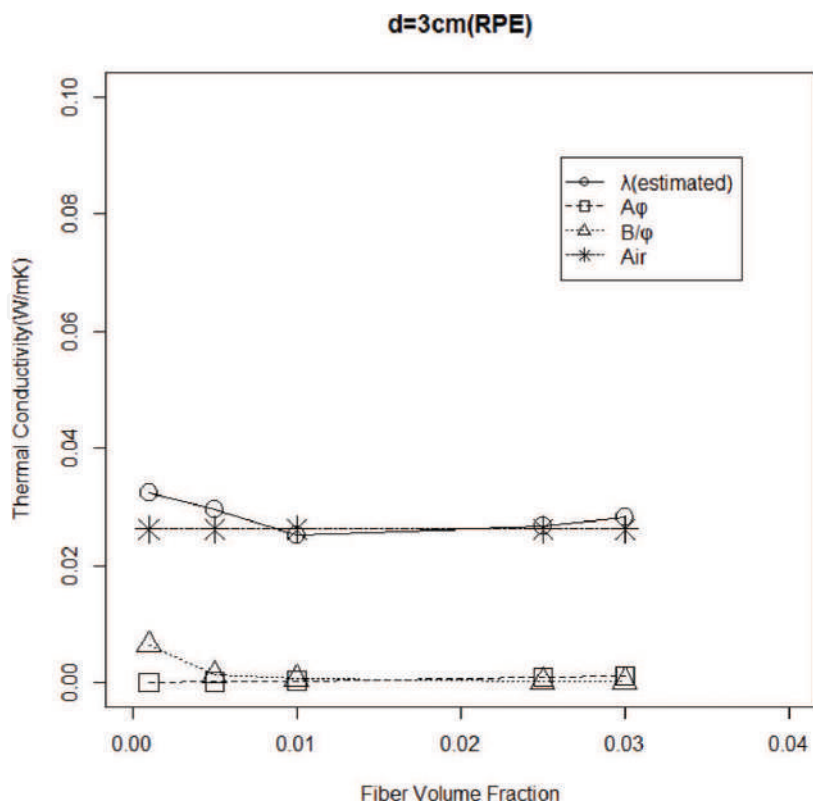


Figure 20. Estimated values of effective thermal conductivity and its component (sample: RPE, d = 3 cm).

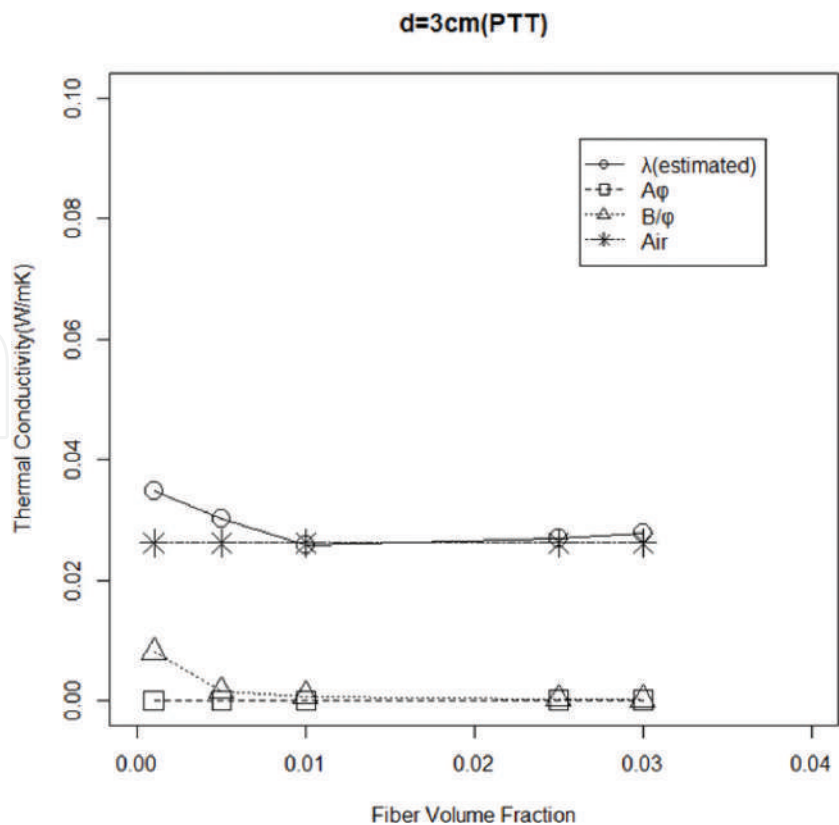


Figure 21. Estimated values of effective thermal conductivity and its component (sample: PTT, d = 3 cm).

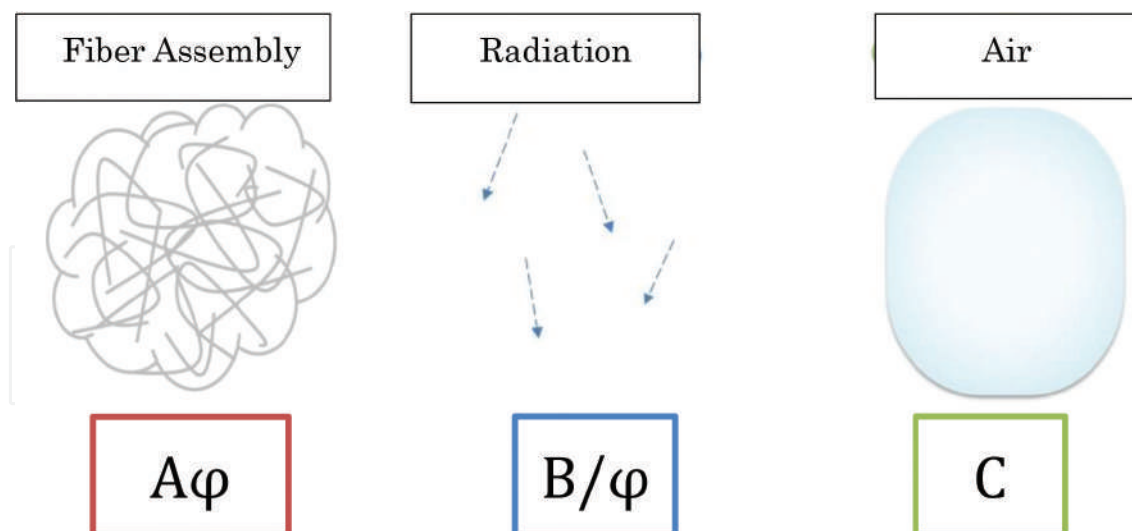


Figure 22. Mechanism of heat transfer in fiber assembly.

contribution of radiative heat transfer is negligible small to effective thermal conductivity of fiber assembly with random orientation. It is conjectured that relative ratio of each heat transfer component depends on fiber material and the effect of pore structure. These findings will be basic information for designing fiber assembly-based thermal insulation material.

6. Conclusion

In this study, the effective thermal conductivity of staple fiber assembly for wadding use is measured. Samples used are four kinds of fiber materials such as cupra fiber (CU), polyester fiber with round section (RPE), polyester fiber with heteromorphic section (WPE), and polytrimethylene terephthalate fiber (PTT).

Effective thermal conductivity is measured under five different fiber volume fractions, and effective thermal conductivity curve is obtained. Effective thermal conductivity curve is analyzed using empirical equation considering separation of heat transfer component. The results are analyzed by nonlinear regression method. Measurement is carried out including leakage of heat from sidewall of the sample frame. Calibration of leakage of heat is accomplished after the separation of heat transfer component by nonlinear regression analysis. Care must be taken so that the measurement system is not disturbed by radiative and convective heat transfer from outer environment. The results obtained are as follows.

1. The shape of effective thermal conductivity-fiber volume fraction curve is convex downward. For CU fiber, the minimum value of effective thermal conductivity lies around $\phi = 0.005$. For polyester fibers (RPE, WPE, PTT), the minimum value lies around $\phi = 0.01$.
2. Effective thermal conductivity can be separated into three components such as conduction in fiber, $A\phi$, radiative heat transfer, B/ϕ , and gas conduction, C .
3. Elimination of leakage of heat is accomplished after the separation of C component into thermal conductivity of air, λ_{air} , and leakage of heat from sidewall, C' .

4. Thermal conductivity of air, λ_{air} , has large contribution to total effective thermal conductivity, and conduction in fiber, $A\phi$ follows in the range of higher fiber volume fraction. Contribution of radiative heat transfer is negligible small through this measurement.
5. Effective thermal conductivity of CU is the largest, and those of polyester fibers (RPE, WPE, PTT) follows.
6. With decreasing thickness, the shape of effective thermal conductivity curve becomes flattened, and the difference between fiber materials becomes small.

Precise determination of C value is required for the precise measurement of effective thermal conductivity. These findings will be basic information for designing fiber assembly-based thermal insulation materials.

A. Appendix: Nonlinear regression model for effective thermal conductivity of fiber assembly

As porosity of fiber assembly in this study is very large (>97%), it is expected that heat transfer within fiber assembly is affected by the effect concerning pore as well as conduction in fiber. Mechanism of heat transfer consists of conduction in fiber, radiative heat transfer in pore, and gas conduction in air. If it is supposed that three components of heat transfer are arranged parallel to heat flux (parallel model), the effective thermal conductivity of fiber assembly, λ (W/mK), is expressed as a function of bulk density ρ (kg/m³) as follows [4].

$$\lambda = \lambda_c + \lambda_r + \lambda_g. \quad (\text{A1a})$$

$$= A\rho + B/\rho + C. \quad (\text{A1b})$$

where λ_c is equivalent thermal conductivity of fiber, λ_r is equivalent thermal conductivity of radiative heat transfer, λ_g is equivalent thermal conductivity of gas conduction, A (Wm²/Kkg) and B (Wkg/m⁴K) are coefficients, and C (W/mK) is constant.

The first term in Eq. (A1b) denotes conduction in fiber, the second term denotes radiative heat transfer, and the third term denotes conductive heat transfer through gas. Here, the physical meaning of parameters A, B, and C are summarized based on literature [4] and other literatures concerning subjects in this study.

A.1. Conduction in fiber

Conduction in fiber consists of two components that is, conduction through fiber and conduction at contact point between fibers. The factors concerning conduction in fibers, therefore, are numbers of fiber and numbers of contact point per unit volume. These factors are expected to be increase with increasing bulk density. If the relation between these factors and bulk density is assumed to be proportional for the simplification, equivalent thermal conductivity for conduction in fiber, λ_c is expressed using coefficient A as follows:

$$\lambda_c = A\rho. \quad (\text{A2})$$

A.2. Radiative heat transfer in pore.

Equivalent thermal conductivity of radiative heat transfer in pore within fiber assembly is expressed as follows:

$$\lambda_r = 4C_0 d\sigma\epsilon T^3. \quad (A3)$$

where C_0 is constant coefficient (n.d.), d is distance between parallel plate (m), σ is Stefan-Boltzmann constant (W/m^2K^4), ϵ is emissivity (n.d.), and T is absolute temperature (K).

Let M be the mass of fiber assembly filled into cell and S be area of section, $d = M/S\rho$. Substituting $M/S\rho$ for d in Eq. (A3), λ_r is expressed as,

$$\lambda_r = 4 C_0 \frac{M}{S\rho} \sigma \epsilon T^3 = \frac{B}{\rho} \quad (A4)$$

$$B = 4 C_0 \frac{M}{S} \sigma \epsilon T^3 \quad (A5)$$

Nogai et al. [1, 2] classifies contribution of total radiative heat transfer in fiber assembly into following four elements: between heat source and fibers, (2) between heat source and heat sink, (3) between fibers, and (4) between fibers and heat sink.

Equation (A3) expresses radiative heat transfer between heat source and heat sink (2).

A.3. Conductive heat transfer through gas

The third term, C (W/mK), is discussed in this section. It is confirmed that size of pore in this experiment is much larger than L , mean free path of air under atmospheric pressure. Therefore, it must be investigated that natural convection occurs or not by change of porosity.

To judge generation of natural convection in fiber assembly, it is not suitable to use Rayleigh number. Instead, modified Rayleigh number [10] to which shape factor of fiber assembly is added is used.

$$Ra = \frac{g\beta\Delta\theta d^3}{\nu\kappa} \frac{k}{d^2} \quad (A6)$$

where g is acceleration of gravity ($=9.8 \text{ m/s}^2$), β is coefficient of body inflation ($1/K$), $\Delta\theta$ is temperature difference between heat source and heat sink (K), d is thickness of sample (m), ν is dynamic viscosity of air (m^2/s), κ is thermal diffusivity of air (m^2/s). k (m^2) is Darcy's transmission coefficient which depends on fiber diameter, t (m) and porosity, ϕ (n.d.).

$$k = \frac{t^2 \phi^3}{122(1-\phi)^2} \quad (A7)$$

If Ra is larger than critical modified Rayleigh number, Ra_{cr} ($=39.5$), natural convection occurs in fiber assembly.

An example of calculation of Ra for sample RPE is shown. Parameters concerning sample RPE ($\phi = 0.03$, $T = 25^\circ\text{C}$) are as follows:

$t = 1.276 \times 10^{-5}$ (m), $\phi = 0.97$, $g = 9.8$ (m^2/s), $\beta = 1/373$ ($1/\text{K}$), $\Delta\theta = 10$ (K), $\nu = 1.579 \times 10^{-5}$ (m^2/s), $\kappa = 2.215 \times 10^{-5}$ (m^2/s).

Ra is calculated as follows:

$$\text{Ra} = 0.0202 \text{ for } d = 0.02$$

$$\text{Ra} = 0.0304 \text{ for } d = 0.03$$

$$\text{Ra} = 0.0513 \text{ for } d = 0.05$$

As $\text{Ra} < \text{Ra}_{\text{cr}}$ ($=39.5$) for all cases, natural convection does not occur in fiber assembly in this case. Therefore, C is constant and $\lambda_g = C$. C is called as component of gas conduction.

Author details

Morihiro Yoneda

Address all correspondence to: gkdzd429@ybb.ne.jp

Nara Women's University, Kitauoya-Nishimachi, Nara, Japan

References

- [1] Nogai T. Estimation of the effective thermal conductivity perpendicular to fiber axes of unidirectionally oriented fiber assembly. *Sen' i-Gakkaishi*. 1980;**36**:389-396
- [2] Nogai T, Ihara M. An experimental study of the effective thermal conductivity perpendicular to fiber axes of unidirectionally oriented fiber assembly. *Sen'i-Gakkaishi*. 1980;**36**:427-434
- [3] Fujimoto T, Niwa M. Experimental study of effective thermal conductivity of fiber assembly Part 1: Evaluation of anisotropic effective thermal conductivity and role of radiative heat transfer. *Journal of Textile Machinery Society of Japan*. 1989;**42**:27-35
- [4] Ohmura T, Tsuboi M, Onodera M, Tomimura T. Study on effective thermal conductivity of fibrous insulation. In: *Proceedings of the Institute for Functional Material Science (Kyusyu University)*. 2002;**16**:13-17
- [5] Rennex B, Somers T. Apparent-thermal-conductivity characterization of low-density, glass-fiber insulation material, *Journal of Thermal Insulation* (predecessor journal of *Journal of Building Physics*). 1985;**8**:175-197
- [6] Symons JG, Clarke RE, Peirce JV. The thermal performance of several Australian fibrous insulating materials. *Journal of Thermal Insulation and Building Envelopes* (predecessor journal of *Journal of Building Physics*). 1995;**19**:72-88

- [7] Campanale M, Moro L. Simplified procedure for the determination of thermal resistance of thick specimens enclosing air only. *Journal of Thermal Insulation and Building Envelopes* (predecessor journal of *Journal of Building Physics*). 1997;**21**:153-170
- [8] Kawabata S. Development of a device for measuring heat-moisture transfer properties of apparel fabrics. *Journal of Textile Machinery Society of Japan*. 1984;**37**:130-138
- [9] Japan Society of Thermophysical Properties, editors. In: *Thermophysical Properties Handbook. Thermophysical Properties of Air*. Tokyo: Yokendo Ltd.; 1990. p.59. ch-B.5.6
- [10] Natural convection heat transfer in porous materials. *Ibid.* p.178. ch-C.2.5.6

IntechOpen

We are IntechOpen, the world's leading publisher of Open Access books Built by scientists, for scientists

6,300

Open access books available

171,000

International authors and editors

190M

Downloads

Our authors are among the

154

Countries delivered to

TOP 1%

most cited scientists

12.2%

Contributors from top 500 universities



WEB OF SCIENCE™

Selection of our books indexed in the Book Citation Index
in Web of Science™ Core Collection (BKCI)

Interested in publishing with us?
Contact book.department@intechopen.com

Numbers displayed above are based on latest data collected.
For more information visit www.intechopen.com



Thermal Conductivity of Liquid Metals

Peter Pichler and Gernot Pottlacher

Additional information is available at the end of the chapter

<http://dx.doi.org/10.5772/intechopen.75431>

Abstract

Over the last decades, many experimental methods have been developed and improved to measure thermophysical properties of matter. This chapter gives an overview over the most common techniques to obtain thermal conductivity λ as a function of temperature T . These methods can be divided into steady state and transient methods. At the Institute of Experimental Physics at Graz University of Technology, an ohmic pulse-heating apparatus was installed in the 1980s, and has been further improved over the years, which allows the investigation of thermal conductivity and thermal diffusivity for the end of the solid phase and especially for the liquid phase of metals and alloys. This apparatus will be described in more detail. To determine thermal conductivity and thermal diffusivity with the ohmic pulse-heating method, the Wiedemann-Franz law is used. There are electronic as well as lattice contributions to thermal conductivity. As the materials examined at Graz University of Technology, are mostly in the liquid phase, the lattice contribution to thermal conductivity is negligibly small in most cases. Uncertainties for thermal conductivity for aluminum have been estimated $\pm 6\%$ in the solid phase and $\pm 5\%$ in the liquid phase.

Keywords: thermal conductivity, ohmic pulse-heating, Wiedemann-Franz law, sub-second physics, high temperature, liquid phase

1. Introduction

Knowing thermophysical properties, i.e., properties that are influenced by temperature, of metals and alloys is not only of academic interest, but also profoundly important for industry and commerce. Casting of metal objects, made of, e.g., steel or aluminum, is prone to casting defects and imperfections. Therefore, in the majority of modern production procedures, computer simulations are performed to reduce defects and imperfections as well as generally

optimize manufacturing processes. The driven benefits from such simulations often are limited by an insufficient or lacking access to experimentally obtained data. It is especially the liquid phase of metals and alloys, that is of interest, as such production processes like, e.g., casting, naturally take place in the liquid phase.

The term thermophysical properties include various properties: thermal conductivity, thermal diffusivity, thermal volume expansion, heat capacity, density, viscosity and so on. Many of those properties are important in industrial processes; however, it is thermal conductivity, more precisely, thermal conductivity of liquid metals and alloys that will be discussed in this chapter.

Naturally, the numbers of experimental methods to measure the desired quantities that have been developed over the past decades are manifold. It is the goal of this work to give a brief overview of the most common or practical techniques in Section 2, but only few of these methods are suitable to conduct measurements in the liquid phase. These techniques will be highlighted in Section 2.

At the Thermo- and Metalphysics group at Graz University of Technology, fast pulse-heating experiments are performed to measure thermophysical properties of liquid metals and alloys. The Wiedemann-Franz law is applied to calculate thermal diffusivity and thermal conductivity from measured quantities. These mentioned calculations are briefly explained in Section 3, and the experimental apparatus used is described in Section 4.

2. An overview of methods to measure thermal conductivity of liquid metals

In principle, there are three different classes of measurement methods:

- Steady state methods
- Non-steady state methods
- Transient methods

However, it is not always as easy to classify a certain technique. Especially, distinguishing between non-steady state methods and transient methods can be challenging.

Steady state methods are defined as techniques, where the temperature gradient remains constant across the sample. Those methods require precise temperature control throughout the whole experiment to confine convection effects to a minimum, which is especially hard to achieve for metals with high melting points.

Transient methods and non-steady state methods make use of very short time frames in order to conclude measurements before convection plays a role. Non-steady state methods achieve those conditions due to very high heating rates of up to 1000 K s^{-1} , with rather large temperature gradients of over 100 K.

The temperature gradient in transient methods is significantly lower (on the order of 5 K) than in non-steady state methods, which minimizes the possibility of convection-induced effects in the measurements. In recent history transient methods grew in importance and started to replace non-steady state methods.

2.1. Steady state methods

2.1.1. Axial heat flow method

A known heat flux q is applied to one end of a sample and dissipated on the other end by a heat sink. Thermal conductivity can be calculated by

$$\lambda = \frac{q}{A} \cdot \frac{\Delta z}{\Delta T} \quad (1)$$

where q is the applied heat flux, A is the specimen cross-section, and $\frac{\Delta z}{\Delta T}$ is the inverse temperature gradient across two points z_1 and z_2 .

Therefore, the conditions to determine thermal conductivity with this method is the determination of the geometry A and Δz , guarantee that the heat flow is unidirectional, measurement of the heat flux q , and measurement of temperature of at least two points z_1 and z_2 (normally thermocouples).

While this technique is mostly targeted at solid materials, it can be used on a variety of liquid metals with low melting points such as mercury, lead, indium, and gallium [1].

The temperature range is 90–1300 K, and the accuracy in this range has been estimated to be ± 0.5 to $\pm 2\%$ [2].

2.1.2. Radial heat flow method

Another method to measure thermal conductivity for both solid and liquid materials is the concentric cylinder method.

The solid sample is placed in-between two concentric cylinders, and a known heat flux is applied by leading a heater through the inner cylinder. The outer cylinder is water cooled to provide a temperature gradient between the two cylinders.

The temperature difference between temperature sensors (often thermocouples) in the two cylinders is determined when steady state is achieved. Knowing the radii of the two cylinders and their length, thermal conductivity can be calculated by

$$\lambda = \frac{q}{L} \cdot \frac{\ln\left(\frac{r_2}{r_1}\right)}{2 \cdot \pi \cdot (T_1 - T_2)} \quad (2)$$

with q being the applied heat flux, L as the length of the cylinders, r_1 as radius of the inner cylinder, r_2 as radius of the outer cylinder, and T_1 and T_2 as the respective temperatures.

A more in-depth explanation of this method can be found in [2].

The method can be adapted for liquid metals by providing a container for the liquid sample in-between the two concentric cylinders. Apart from this container, the measuring principle remains the same for liquid metal samples.

The radial heat flow method operates in a temperature range of 4–1000 K and the uncertainty of this method has been estimated to be about $\pm 2\%$ [3].

2.2. Direct heating methods

The term “direct electrical heating method” summarizes all those measurement techniques, where the sample is heated up, by running a current through it, without an additional furnace. An example of such a method, but in a dynamic way and not as a steady state method, is the ohmic pulse-heating method that will be discussed later in this chapter.

Direct electrical heating methods are therefore limited to samples which are decent electrical conductors. The shape of the samples can vary from wires, rods, sheets to tubes. The advantage of such techniques is for one, the lack of a furnace and, secondly, the possibility to measure a multitude of thermophysical properties simultaneously.

Direct heating methods are able to achieve high temperatures of about 4000 K and are therefore suitable for measuring thermal conductivity in the liquid phase of metals with high melting points.

2.2.1. Guarded hot plate

This steady state method utilizes two temperature-controlled plates that sandwich a solid disc-shaped sample. Heating one plate, while cooling the other one, generates a uniformly distributed heat flux through the sample, achieving a steady state temperature at each plate. The technique is considered as the steady state method with the highest accuracy.

The guarded hot plate apparatus can be constructed in single sided or double sided mode. When operated in double sided mode, there is a total amount of three plates as well as two samples: A central heater plate together with two cooling plates sandwiching the two samples. The temperature drop across the two specimens is measured with thermocouples, which are apart a distance L . Thermal conductivity can then be determined by

$$\lambda = \frac{q \cdot L}{2 \cdot A \cdot \Delta T} \quad (3)$$

where q is the heat flux through the specimen, A is the cross section, L is the spatial distance between the two thermocouples, and ΔT is the temperature difference.

In the single-sided mode, one of the cooling plates as well as the second specimen is removed. The temperature gradient in one direction therefore vanishes, which leads to the loss of a factor 2 in Eq. (3)

$$\lambda = \frac{q \cdot L}{A \cdot \Delta T} \quad (4)$$

The experimental setup and the calculation of the thermal conductivity are more thoroughly explained in [4].

Commercially available guarded hot plate (GHP) apparatus, like the NETZSCH GHP 456 Titan [5], operate in a temperature range of 110–520 K and provide an accuracy of $\pm 2\%$.

It has to be noted that the GHP method is applicable only for solid samples and it is not a suitable method to determine thermal conductivity of high-melting metals.

2.2.2. Calorimeter method

The calorimeter technique is a direct measurement of Fourier's law. It consists of a heating source (typically SiC or MoSi₂ elements) and a SiC slab to distribute the temperature gradient. The specimen is enclosed by two insulating guard bricks, which are, like the specimen as well, in thermal contact with a water-cooled copper base. As the name gives away, the central part of the system is a calorimeter, which is surrounded by the guards. The apparatus is designed in a way that the heat flow into the calorimeter is one-dimensional.

Two thermocouples, which are apart a distance L and lie vertically to each other, are enclosed in the specimen and the temperature difference $T_2 - T_1$ between them is measured.

Thermal conductivity can be determined by

$$\lambda = \frac{\frac{dq}{dt} \cdot L}{A(T_2 - T_1)} \quad (5)$$

with A being the cross section of the calorimeter, L as the distance between the two thermocouples, $\frac{dq}{dt}$ as the rate of heat flow into the calorimeter, and $T_2 - T_1$ as the temperature difference between the two thermocouples.

2.3. Transient methods

2.3.1. Transient hot wire and transient hot strip method

Simple experimental arrangements and short measurement times are granted by the transient hot wire (THW) along with the transient hot strip (THS) method.

The transient hot wire technique is most commonly used for measuring thermal conductivity λ and thermal diffusivity a . An electrically heated wire, which acts as a self-heated thermometer is placed into a material and distributes a radial heat flow into the sample. The specimen itself acts as a heat sink for the system, while the wire functions as a heat source as well as providing a mechanism to measure the thermal transport properties, due to a temperature-dependent drop of the voltage along the wire. Solving the fundamental heat conduction equation yields

$$\Delta T(r, t) = \frac{q}{4 \cdot \pi \cdot \lambda} \cdot \ln\left(\frac{4 \cdot a \cdot t}{r^2 \cdot e^\gamma}\right), \quad (6)$$

with q the heat input per unit length of the wire, r the radius of the wire, a the thermal diffusivity, γ Euler's constant, t the time, and λ , of course, the thermal conductivity.

An in-depth explanation of this method to determine thermal conductivity is given in [6, 7].

The transient hot strip (THS) method further improves the THW method. Instead of a wire as the heat source and measuring device, a thin strip of metal foil is used. The metal foil provides a greater surface as well as a smaller thickness than the heated wire, leading to a lower density of heat flow and consequently, a smaller thermal contact resistance to the sample.

While the THW method is only applicable for liquids and some solids, which can be wrapped around the heating wire in a way the thermal resistance is low enough, the THS method is the go-to method to perform measurements on solids.

Note: this work focuses on the measurement techniques for thermal conductivity of liquids. THS measurements are also performed on gases (see [8]).

At Physikalisch-Technische Bundesanstalt (PTB), Braunschweig, an upgraded version of the THS and THW method, the transient hot bridge technique, has been developed. In this method, a total of eight strips are deployed in a way they form a Wheatstone bridge, allowing an effective thermal and electrical self-compensation [9].

Uncertainties of the THW technique have been reported (e.g., see [10]) to be $\pm 5.8\%$ for the determination of thermal conductivity. However, the method has also been described as even more accurate [11], with uncertainties of below $\pm 1\%$ for gases, liquids, and solids. With a maximum temperature of about 1000 K, this method is only suitable for low melting metals.

2.3.2. 3ω method

The 3ω method goes back to the work done by Cahill [12] in 1987. The method has similarities with the THS and THW technique, since it also uses a single element as heat source as well as thermometer. While both the THS and THW method measure temperature in dependence of time, the 3ω technique records the amplitude and phase of the resistance depending on the frequency of the excitation.

It is most commonly used as a technique to measure thermal conductivity of solids or liquids, but has been improved to also be applicable on thin films [12, 13]. A conducting wire is distributed onto a specimen and an AC voltage with a frequency ω is driven through it. Due to the electrical resistance, the sample is heated up, resulting in a temperature change. The frequency of the change in temperature is 2ω . The product of the resistance oscillation 2ω and the excitation frequency ω gives a voltage of frequency 3ω , which is measured and responsible for the name 3ω method.

Measuring the 3ω voltage at two frequencies f_1 and f_2 , thermal conductivity is

$$\lambda = \frac{V^3 \ln f_2 / f_1}{4 \cdot \pi \cdot l \cdot R^2 (V_{3,1} - V_{3,2})} \frac{dR}{dT} \quad (7)$$

with $V_{3,1}$ the 3ω voltage at frequency f_1 , $V_{3,2}$ the 3ω voltage at frequency f_2 , and R the average resistance of the metal line of length l .

In the original work of Cahill [13], the temperature range of the 3ω method is 30–750 K, which is not suitable for high melting metals. This method often is applied on nanofluids and publications state an uncertainty of around $\pm 2\%$ [14].

2.3.3. Laser flash method

Under the laser flash method (LFM), the directly measured quantity is thermal diffusivity and not thermal conductivity. Thermal conductivity can, however, be determined with knowledge of specific heat as well as density of the sample.

$$\lambda(T) = a(T) \cdot \rho(T) \cdot c_p(T), \quad (8)$$

with $a(T)$ the thermal diffusivity, $\rho(T)$ the density, and $c_p(T)$ the specific heat.

In the LFM, the sample is exposed to a high intensity laser pulse at one face, which generates heat at said surface. On the back surface, which is not exposed to the laser pulse, an infrared sensor detects a rising temperature signal, due to heat transfer through the sample.

For adiabatic conditions, thermal diffusivity can be obtained by

$$a = 0.1388 \frac{l^2}{t_{0.5}}, \quad (9)$$

with l the sample thickness and $t_{0.5}$ the time at 50% of the temperature increase.

LFM, as introduced by Parker et al. [15], has been a convenient technique to determine thermal diffusivity a and thermal conductivity λ of solids at moderate temperatures. The method has been further improved since then and is applicable for a great temperature range, up to around 2500°C.

In 1972, Schriempf [16] applied LFM to determine thermal diffusivity for liquid metals at high temperatures. The liquid metal has to be placed in a suitable container in order to arrange a proper setup. Problems arise for liquids of low thermal conductivity. When the thermal conductivity of the sample is of the same order as of the container, this leads to an unneglectable heat current through the container. Therefore, it was proposed in [17] not to insert the liquid sample into a container, but have it placed between a metal disc, which is exposed to the laser pulse.

Commercially available laser flash apparatus like the NETZSCH LFA 427 [18] operate in a temperature range from -120 to 2800°C , depending on the furnace and are therefore applicable for higher melting metals as well.

Kaschnitz [19] estimates uncertainties of thermal conductivity for LFM to be between ± 3 and $\pm 5\%$ in the solid phase and ± 8 to $\pm 15\%$ in the liquid phase.

Hay [20] did an uncertainty assessment for their apparatus at Bureau national de métrologie (BNM) and claimed uncertainty estimations from ± 3 to $\pm 5\%$.

Hohenauer [21] did an uncertainty assessment of their laser flash apparatus and stated an expanded uncertainty with thermal diffusivity measurement in the temperature range from 20 to 900°C of 3.98%.

3. Calculations via Wiedemann-Franz law

In some cases, it is more applicable to measure electrical conductivity respectively electrical resistivity. Heat transport and thus thermal conductivity through a metal or an alloy needs carriers. One has to distinguish between the component λ_e of thermal conductivity due to electrons and λ_l , which is the lattice contribution, due to phonons. Naturally for liquid metals and alloys, thermal conductivity is dominated by the electronic contribution. The total thermal conductivity would then be the sum of the components $\lambda = \lambda_e + \lambda_l$.

Thermal conductivity of liquid aluminum was examined at Graz University of Technology. Here the sole consideration of the electronic contribution gave promising results for the liquid phase [22]. A detailed derivation of the lattice-contribution to thermal conductivity can be found in the paper of Klemens [23].

An example when the lattice contribution has to be considered in the calculation of thermal conductivity for the Inconel 718 alloy is given in [24].

The Wiedemann-Franz law states that for conducting metals the electronic component of the thermal conductivity λ_e is

$$\lambda_e = L_0 \frac{T}{\rho(T)} \quad (10)$$

with $\rho(T)$ the temperature-dependent electrical resistivity and $L = \frac{\pi^2}{3} \cdot (k_B/e)^2 = 2.45 \times 10^{-8} \text{ W} \cdot \Omega \cdot \text{K}^{-2}$ the (theoretical) Lorenz number.

Considering thermal expansion, the temperature-dependent electrical resistivity is

$$\rho(T) = \rho_{IG} \frac{d(T)^2}{d_0^2}, \quad (11)$$

with d_0 the diameter at reference temperature (room temperature), ρ_{IG} the electrical resistivity at initial geometry, and $d(T)$ the diameter at an elevated temperature T . To calculate thermal conductivity, it is therefore necessary to measure thermal volume expansion as well.

An estimation of thermal diffusivity $a(T)$ can be found by

$$a(T) = \frac{L_0 \cdot T}{c_p(T) \cdot D(T) \cdot \rho(T)} \quad (12)$$

with $c_p(T)$ the heat-capacity and $D(T)$ the temperature-dependent density. With the ohmic pulse-heating setup at Graz University of Technology (as explained later in this work), radial over longitudinal expansion is ensured (see, e.g., [25]). Considering Eq. (12) and radial expansion yields

$$a(T) = \frac{L_0 \cdot T}{c_p(T) \cdot D(T) \cdot \rho(T)} = \frac{L_0 \cdot T}{c_p(T) \cdot D_0 \cdot \rho_{IG}} \quad (13)$$

with D_0 the density at room temperature.

Thus, Eqs. (10) and (12) enable us to determine thermal conductivity and thermal diffusivity from ohmic pulse-heating experiments, and deliver results that are in the same range as results from Laser flash measurements, as shown in the thermal diffusivity intercomparisons NPL – Report CBTLM S30 [26]. With a variation of only 3%, our results were significantly close to the average determined.

The experimental setup at Graz University of Technology is described in the following section.

4. Measurements at Graz University of Technology

In ohmic pulse-heating experiments, the electric conducting sample is heated up by passing a large current pulse through it. Due to the resistivity of the material, the sample is heated up from room temperature to the melting point and further up through the liquid phase to the boiling point in a period of about 50–70 μ s.

The specimen typically is in the shape of a wire, with diameters ranging from a few hundred micrometers up to some millimeters, rectangular shape for materials that cannot be drawn into wires, foils or tubes. As a consequence of the narrow time frame under which these experiments are performed, the liquid phase does not collapse due to gravitational forces, enabling investigations of the entire liquid phase up to the boiling point. In addition, the specimen can be considered to not be in contact with the surrounding medium, rendering the experiment to being a container-less method.

4.1. Setup

A typical pulse heating experiment consists of the following parts: An energy storage (mostly a capacitor or battery bank) with a charging unit, a main switching unit (e.g., high-voltage mercury vapor ignition tubes) and an experimental chamber with windows for optical diagnostics and the ability to maintain a controlled ambient atmosphere. Pulse heating experiments are mostly performed under inert atmosphere, e.g., nitrogen or argon at ambient pressure,

or in vacuum. The setup of the pulse-heating apparatus at Graz University of Technology is presented in **Figure 1**.

The setup has been explained in detail in previous publications [27–29].

4.2. Current and voltage measurement

The current pulse, which the sample is subjected to, is measured using an induction coil (Pearson Electronics, Model Number 3025). To measure the voltage drop, two Molybdenum voltage-knives are attached to the specimen. The voltage drop relative to a common ground is measured for both of the voltage-knives, allowing the measurement of the voltage drop between the two contact points of the sample and the respective voltage-knives (**Figure 2**).

4.3. Temperature measurement

A fast pyrometer provides temperature determination. The pyrometer measures the spectral radiance of a sample surface from which the temperature can be calculated using Planck's law.

$$L_{\lambda,B}(\lambda, T) = \frac{c_1}{\pi \cdot \lambda^5} \cdot \frac{1}{e^{\frac{c_2}{\lambda T}} - 1} \quad (14)$$

with $L_{\lambda,B}(\lambda, T)$ the radiance emitted by a black body at temperature T and wavelength λ and the two radiation constants $c_1 = 2\pi \cdot h \cdot c^2$ and $c_2 = \frac{h \cdot c}{k_B}$ (h is the Planck's constant, c the speed of light, and k_B the Boltzmann constant). It has to be considered that nearly no real material is a perfect black body. The deviation from black body radiation is taken into account by emissivity $\varepsilon(\lambda, T)$. The ratio of radiation emitted by a real material therefore is

$$L_{\lambda}(\lambda, T) = \varepsilon(\lambda, T) \cdot L_{\lambda,B}(\lambda, T). \quad (15)$$

It has to be noted as well that the measured quantity of the pyrometer is a voltage signal $U_{pyro}(T)$, which is dependent on measuring geometry, transmission of the optical measuring setup, width of the spectral range and detector sensitivity. When summarizing the majority of the temperature-independent quantities in a constant C , the pyrometer signal is

$$U_{pyro}(T) = C \cdot \varepsilon(\lambda, T) \cdot \left(e^{\frac{c_2}{\lambda T}} - 1\right)^{-1} \quad (16)$$

4.4. Thermal diffusivity and thermal conductivity

With the obtained values of the time-dependent current $I(t)$, the time-dependent voltage drop $U(t)$, the specimen radius $r(t)$ and the surface radiation $L(t)$ it is now possible to calculate the desired thermal properties, i.e., thermal conductivity $\lambda(T)$, thermal diffusivity $a(T)$ as well as specific heat capacity $c_p(T)$. This has been shown briefly in the second section of this chapter and is thoroughly discussed in [30, 31].

The solid phase as well as the liquid phase data are fitted linearly (for the solid phase) and quadratically (for the liquid phase). In our publications (e.g., [22]) we give the coefficients for the

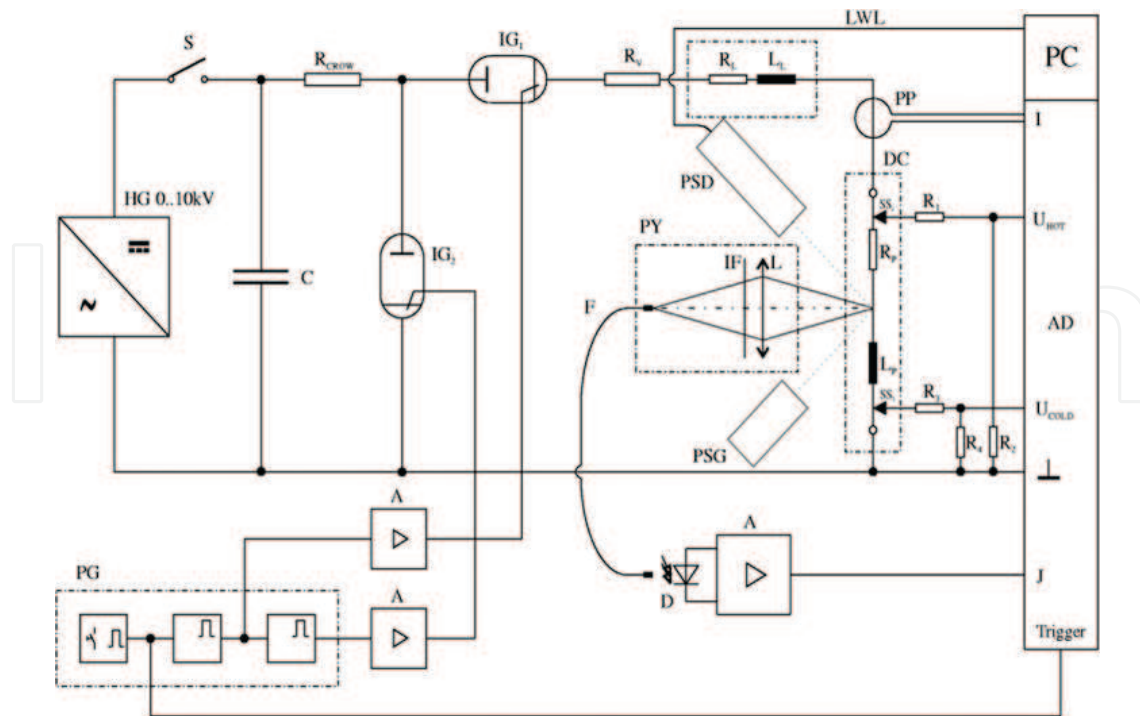


Figure 1. Schematic experimental setup. HG: high voltage power supply; S: switch for loading the capacitor bank C; R CROW: crowbar resistor; IG 1: main ignitron; IG 2: crowbar ignitron; R V: matching resistor; R C, L C, R S, L S: resistance and inductance of the circuit and/or the sample; R 1 – R 4: voltage dividers; K E 1, K E 2: knife-edge probes; PP: Pearson-probe; DC: discharge chamber; PY: Pyrometer; L: lens; IF: interference filter; F: fiber; D: photo-diode; A: amplifier; PG: pulse generator; AD: analog-to-digital converter; PC: personal computer; I, U HOT, U COLD, J: measurement signals of current, voltages and intensity of radiation; PSG: polarization state generator; PSD: polarization state detector; LWL: light wire line.

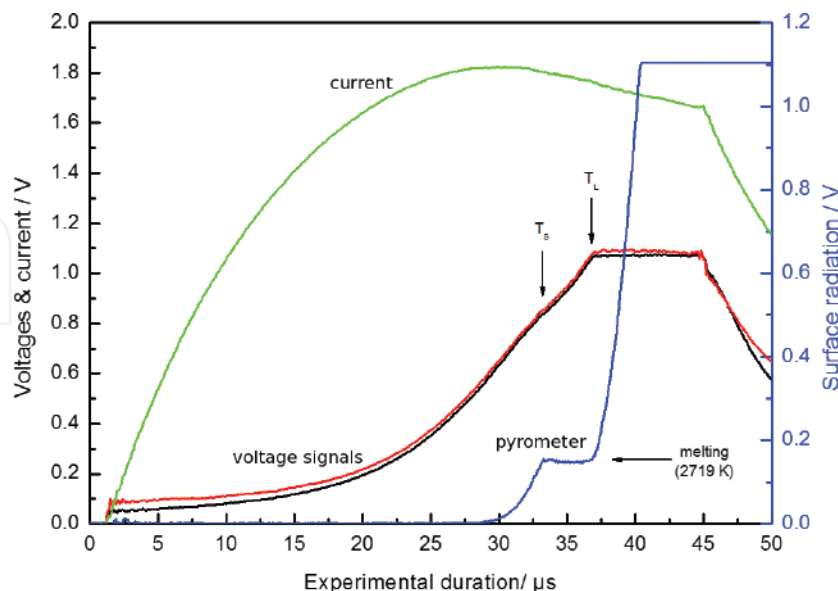


Figure 2. Typical raw measurement signals of the ohmic pulse-heating experiment performed on Iridium. The black line and red line are the voltage signals, the green line is the current signal and the blue line is the signal of the pyrometer. Note that solidus temperature (T_s) and liquidus temperature (T_l) are visible not only in the pyrometer signal, but also in the voltage signals.

linear fits as well as uncertainty assessments. The schematic data provided in this chapter are for aluminum; therefore, the temperature range is rather low. With the ohmic pulse-heating apparatus, it is also possible to examine high melting metals like tungsten, niobium and tantalum.

Figures 3 and **4** show typical results of thermal conductivity and thermal diffusivity determination with the ohmic pulse-heating apparatus for aluminum.

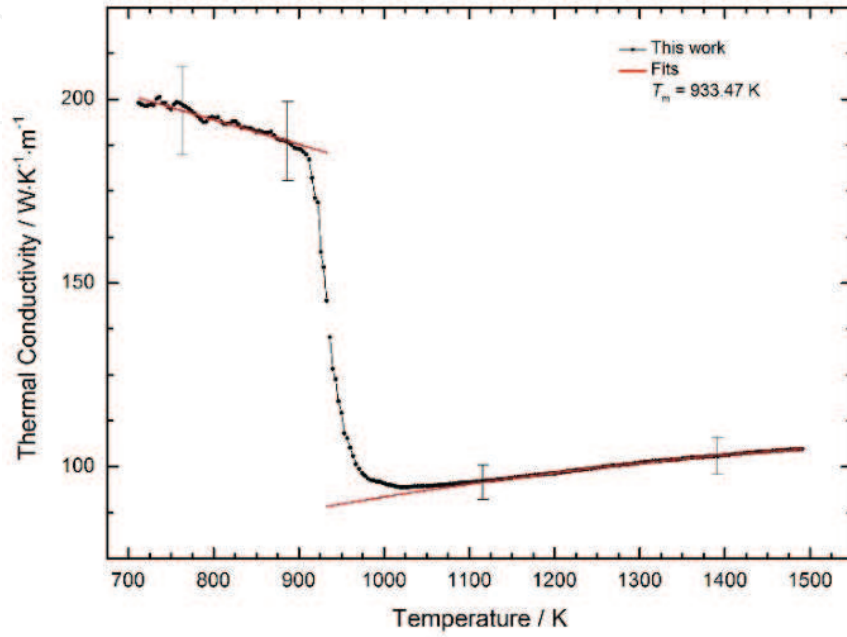


Figure 3. Results of thermal conductivity determination for aluminum. Data taken from [22].

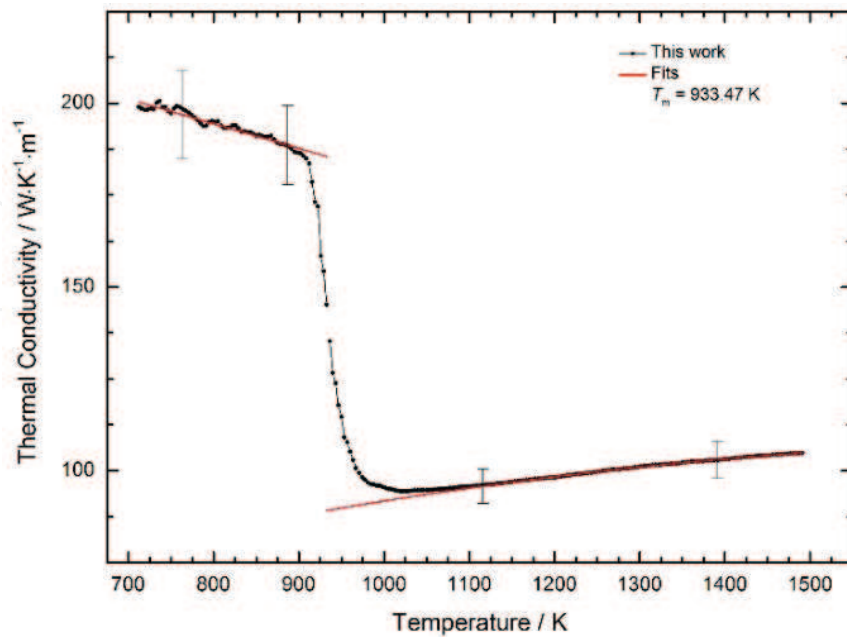


Figure 4. Results of thermal diffusivity determination for aluminum. Data taken from [22].

The data show the solid phase (up to about 900 K) and the liquid phase (up to 1500 K). Thermal conductivity in this case can be fitted quadratically with a positive slope in the liquid phase.

4.5. Uncertainty for the ohmic pulse-heating method

Uncertainties have been estimated according to GUM [32], with a coverage factor of $k = 2$ (95%).

Uncertainties for thermal conductivity $\lambda(T)$ for aluminum have been estimated $\pm 6\%$ in the solid phase and $\pm 5\%$ in the liquid phase. Uncertainties for thermal diffusivity $a(T)$ for aluminum have been estimated $\pm 8\%$ in the solid phase and $\pm 5\%$ in the liquid phase. See also [22].

5. Conclusions

A variety of common methods to determine thermal conductivity of liquid metals have been reviewed in this chapter. These methods can be classified into steady state, non-steady state, and transient techniques. However, not all of the reviewed methods are suitable for the liquid phase of high-melting metals.

To conclude this chapter, the methods that are suitable for the determination of thermal conductivity of high-melting metals in the liquid phase are summarized.

The laser flash method (LFM) is applicable also for high-melting metals, as the temperature range has been reported to be -120 to 2800°C . Uncertainties for this measurement technique range from ± 3 to $\pm 15\%$ [16–19].

Another suitable method to determine thermal conductivity of even high-melting metals in the liquid phase is the ohmic pulse-heating method in combination with the Wiedemann-Franz law. This method can easily achieve temperatures of about 4000 K and higher and is therefore suitable for all high-melting metals (the metal with the highest melting point is tungsten with 3695 K). Uncertainties for thermal conductivity for aluminum have been estimated $\pm 6\%$ in the solid phase and $\pm 5\%$ in the liquid phase [22].

Especially in the liquid phase, where lattice contributions in the determination of thermal conductivity can be neglected, the ohmic pulse-heating method has been proven to be a very accurate method. This has been shown in an intercomparison with laser flash measurements in [26].

Author details

Peter Pichler and Gernot Pottlacher*

*Address all correspondence to: pottlacher@tugraz.at

Institute of Experimental Physics, Graz University of Technology, NAWI Graz, Austria

References

- [1] Mills KC, Monaghan BJ, Keene BJ. Thermal conductivities of molten metals: Part 1. Pure metals. *International Materials Review*. 1996;**41**(6):209-242
- [2] Maglic KD, Cezairliyan A, Peletsky VE. *Compendium of Thermophysical Property Measurement Methods: Vol. 1. Survey of Measurement Techniques*. New York, NY: Plenum Press; 1984
- [3] Buck W, Rudtsch S. Thermal properties. In: Czichos H, Saito T, Smith L, editors. *Springer Handbook of Materials Measurement Methods [Internet]*. Berlin, Heidelberg: Springer Berlin Heidelberg; 2006. pp. 399-429. DOI: 10.1007/978-3-540-30300-8_8
- [4] Salmon D. Thermal conductivity of insulations using guarded hot plates, including recent developments and sources of reference materials. *Measurement Science and Technology*. 2001;**12**(12):R89. Available from: <http://stacks.iop.org/0957-0233/12/i=12/a=201>
- [5] [Internet] [cited 2018/01/20]. Available from: <https://www.netzsch-thermal-analysis.com/en/products-solutions/thermal-diffusivityconductivity/ghp-456-titan/>
- [6] Assael MJ, Dix M, Gialou K, Vozar L, Wakeham WA. Application of the transient hot-wire technique to the measurement of the thermal conductivity of solids. *International Journal of Thermophysics*. 2002;**23**(3):615-633. DOI: 10.1023/A:1015494802462
- [7] Hammerschmidt U. A quasi-steady state technique to measure the thermal conductivity. *International Journal of Thermophysics*. 2003;**24**(5):1291-1312. Available from: <http://link.springer.com/article/10.1023/A:1026151101668>
- [8] Roder HM, Perkins RA, Laesecke A, de Castro CAN. Absolute steady-state thermal conductivity measurements by use of a transient hot-wire system. *Journal of Research of the National Institute of Standards and Technology*. 2000;**105**(2):221
- [9] Hammerschmidt U, Meier V. New transient hot-bridge sensor to measure thermal conductivity, thermal diffusivity, and volumetric specific heat. *International Journal of Thermophysics*. 2006;**27**(3):840-865. DOI: 10.1007/s10765-006-0061-2
- [10] Hammerschmidt U, Sabuga W. Transient hot wire (THW) method: Uncertainty assessment. *International Journal of Thermophysics*. 2000;**21**(6):1255-1278. Available from: <http://link.springer.com/article/10.1023/A:1006649209044>
- [11] Assael MJ, Antoniadis KD, Wakeham WA. Historical evolution of the transient hot-wire technique. *International Journal of Thermophysics*. 2010 Jun 1;**31**(6):1051-1072. DOI: 10.1007/s10765-010-0814-9
- [12] Cahill DG, Katiyar M, Abelson J. Thermal conductivity of a-Si: H thin films. *Physical Review B*. 1994;**50**(9):6077
- [13] Cahill DG. Thermal conductivity measurement from 30 to 750 K: The 3ω method. *Review of Scientific Instruments*. 1990;**61**(2):802-808

- [14] Choi TY, Maneshian MH, Kang B, Chang WS, Han CS, Poulikakos D. Measurement of the thermal conductivity of a water-based single-wall carbon nanotube colloidal suspension with a modified 3- ω method. *Nanotechnology*. 2009;**20**(31):315706. Available from: <http://stacks.iop.org/0957-4484/20/i=31/a=315706>
- [15] Parker W, Jenkins R, Butler C, Abbott G. Flash method of determining thermal diffusivity, heat capacity, and thermal conductivity. *Journal of Applied Physics*. 1961;**32**(9):1679-1684. Available from: <http://scitation.aip.org/content/aip/journal/jap/32/9/10.1063/1.1728417>
- [16] Schriempf JT. A Laser Flash Technique for Determining Thermal Diffusivity of Liquid Metals at Elevated Temperatures. *Review of Scientific Instruments*. 1972;**43**(5):781-786. DOI: 10.1063/1.1685757
- [17] Tada Y, Harada M, Tanigaki M, Eguchi W. Laser flash method for measuring thermal conductivity of liquids—Application to low thermal conductivity liquids. *Review of Scientific Instruments*. 1978;**49**(9):1305-1314
- [18] <https://www.netzsch-thermal-analysis.com/en/products-solutions/thermal-diffusivity-conductivity/lfa-427/> [Internet]. Available from: <https://www.netzsch-thermal-analysis.com/en/products-solutions/thermal-diffusivity-conductivity/lfa-427/>
- [19] Kaschnitz E. Private conversation
- [20] Hay B, Filtz JR, Hameury J, Rongione L. Uncertainty of thermal diffusivity measurements by laser flash method. *International Journal of Thermophysics*. 2005 Nov 1;**26**(6):1883-1898. DOI: 10.1007/s10765-005-8603-6
- [21] Vozár L, Hohenauer W. Uncertainty of thermal diffusivity measurements using the laser flash method. *International Journal of Thermophysics*. 2005 Nov 1;**26**(6):1899-1915. DOI: 10.1007/s10765-005-8604-5
- [22] Leitner M, Leitner T, Schmon A, Aziz K, Pottlacher G. Thermophysical properties of liquid aluminum. *Metallurgical and Materials Transactions A*. 2017;**48**:3036-3045
- [23] Klemens PG, Williams RK. Thermal conductivity of metals and alloys. *International Metals Reviews*. 1986;**31**(5):197-215
- [24] Pottlacher G, Hosaeus H, Kaschnitz E, Seifert A. Thermophysical properties of Inconel 718 alloy up to 1800 celsius. *Scandinavian Journal of Metallurgy*. 2002;**31**:161-168
- [25] Schmon A. Density Determination of Liquid Metals by Means of Containerless Techniques [Internet]. Graz University of Technology; 2016. Available from: https://www.tugraz.at/fileadmin/user_upload/Institute/IEP/Thermophysics_Group/Files/Diss-SchmonAlexander.pdf
- [26] James M, Monaghan B, Cusco L, Redgrove JPQ. Intercomparison of measurements of the thermal diffusivity of molten metals. NPL Report CBTLM S30; 2000
- [27] Cagran C, Huepf T, Wilthan B, Pottlacher G. Selected thermophysical properties of Hf-3% Zr from 2200K to 3500K obtained by a fast pulse-heating technique. *High Temperatures-High Pressures*. 2008;**37**:205-219

- [28] Schmon A, Aziz K, Luckabauer M, Pottlacher G. Thermophysical properties of Manganin ($\text{Cu}_{86}\text{Mn}_{12}\text{Ni}_2$) in the solid and liquid state. *International Journal of Thermophysics*. 2015
- [29] Wilthan B, Cagran C, Brunner C, Pottlacher G. Thermophysical properties of solid and liquid platinum. *Thermochimica Acta*. 2004;**415**:47-54
- [30] Cagran C, Wilthan B, Pottlacher G, Roebuck B, Wickins M, Harding RA. Thermophysical properties of a Ti-44%Al-8%Nb-1%B alloy in the solid and molten states. *Intermetallics*. 2003;**11**:1327-1334
- [31] Kaschnitz E, Pottlacher G, Jaeger H. A new microsecond pulse-heating system to investigate thermophysical properties of solid and liquid metals. *International Journal of Thermophysics*. 1992 Jul;**13**(4):699-710. Available from: <http://www.springerlink.com/openurl.asp?genre=article&id=doi:10.1007/BF00501950>
- [32] Metrology (JCGM/WG 1) WG 1 of the Joint Committee for Guides. In: *Guide to the Expression of Uncertainty in Measurement*. BIPM; 1993

We are IntechOpen, the world's leading publisher of Open Access books Built by scientists, for scientists

6,300

Open access books available

171,000

International authors and editors

190M

Downloads

Our authors are among the

154

Countries delivered to

TOP 1%

most cited scientists

12.2%

Contributors from top 500 universities



WEB OF SCIENCE™

Selection of our books indexed in the Book Citation Index
in Web of Science™ Core Collection (BKCI)

Interested in publishing with us?
Contact book.department@intechopen.com

Numbers displayed above are based on latest data collected.
For more information visit www.intechopen.com



Thermal Conductivity Measurement of the Molten Oxide System in High Temperature

Youngjae Kim, Youngjo Kang and Kazuki Morita

Additional information is available at the end of the chapter

<http://dx.doi.org/10.5772/intechopen.76018>

Abstract

In spite of practical importance in the pyro-metallurgy process, thermal conductivity of molten oxide system has not been sufficiently studied due to its notorious convection and radiation effects. By an aid of appropriate modification of measurement technique and evaluations for systematic errors, thermal conductivity measurement at high temperature becomes feasible. In this chapter, thermal conductivity measurement technique for high-temperature molten oxide system was discussed along with related experimental errors. In addition, thermal conduction mechanism by phonon was briefly introduced. The laser flash method and hot-wire method, which are representative measurement methods for high-temperature system, were compared. During the measurement by using hot-wire method, the convection and radiation effects on measurement results were evaluated. In the hot-wire method, both convection and radiation effects were found to be negligible within short measurement time. Finally, the effect of network structure of molten oxide system on thermal conductivity was discussed. The positive relationship between thermal conductivity and polymerization in the silicate and/or borate system was presented. In addition, the effect of cation expressed by function of ionization potential on thermal conductivity was also briefly introduced. This chapter is partially based on a dissertation submitted by Youngjae Kim in partial fulfillment of the requirements for the degree of Doctor of Philosophy at The University of Tokyo, September 2015.

Keywords: thermal conductivity, hot-wire method, transient method, molten oxide, network structure

1. Introduction

In the iron-making and steel-making field, understanding of thermal conductivity of the molten oxide system is significant because it is closely related with the operation conditions, quality of final products and recycling of slag.

For the recycle of blast furnace slag, the slag is slowly cooled down in the atmosphere or rapidly quenched by using rotary cup atomizer or air blast method. Highly crystallized slag can be recycled as cement concrete for road construction or fertilizer. On the other hand, noncrystalline blast furnace slag can be used as Portland cement for construction owing to its properties of cement when it is ground [1]. Therefore, in order to recycle the blast furnace slag as Portland cement, proper fineness and glass state should be achieved. Since the characteristic fine-granular shape and glass state are mainly determined by a cooling rate, understanding of thermal conductivity of blast furnace slag is important. For this reason, the thermal conductivity measurement in the molten $\text{CaO-SiO}_2\text{-Al}_2\text{O}_3$ system, which is the typical blast furnace slag system, has been carried out by using hot-wire method [2–4] and laser flash method [5].

During the steel-making process, understanding of thermal conductivity of the molten slag is closely related to the quality of final products and refractory lifetime. Recently, many works have been focused on the development of heat flow of the whole steel-making chain. However, due to the short information concerning about thermal conductivity of ladle slag, ladle slag is hardly considered during the simulation [6]. For the purpose of better understanding of heat flow, understanding of thermal conductivity of ladle slag is important. Glaser and Sichen [6] measured thermal conductivity of the conventional ladle slag system; $\text{CaO-SiO}_2\text{-Al}_2\text{O}_3\text{-MgO}$ system, using the hot-wire method. Their results show the negative temperature dependence of thermal conductivity within the experimental region between 1773 and 1923 K. They reported that the formation of solid state in the slag results in the significant increase of thermal conductivity. On the other hand, Kang et al. [7], who measured thermal conductivity in the steel-making slag system of $\text{CaO-SiO}_2\text{-FeO}_x$ system, reported that addition of FeO_x results in the decreasing of thermal conductivity due to the basic oxide behavior of FeO_x . Considering the structural information of FeO_x obtained by Mössbauer, they found the linear relationship between thermal conductivity and the NBO/T , which is the relative fraction of the number of nonbridging oxygen over total tetrahedral cation, implying the effect of network structure on thermal conductivity.

In addition, during the continuous casting process, irregular horizontal heat transfer through mold flux results in the “longitudinal cracking” and “star cracking” on the final product. Therefore, understanding of thermal conductivity of mold flux system is practically important in terms of quality control. Many studies [8–11] have been carried out in order to find out the relationship between structure of mold flux system and thermal conductivity at high temperature of molten state. These works [8–11] commonly observed the structure dependence of thermal conductivity. Addition of basic oxide, such as sodium oxide or calcium oxide, decreases thermal conductivity as a result of depolymerization of silicate network structure [8, 11]. Susa et al. [10] found that fluorides play a role of network modifier resulting in the lowering thermal conductivity. According to Mills [12], phonon transfer along silicate network

chain or ring has much lower thermal resistivity($1/\lambda$) than from chain to chain. Similarly, Susa et al. [10] observed that more ionic bonding has the greater thermal resistivity. Therefore, it can be concluded that the positive relationship between thermal conductivity and network structure is closely related to the formation of covalent bond which has low thermal resistivity.

Not only the steel-making process, but also other pyro-metallurgy process, understanding of thermal conductivity is significant. During the operation of submerged arc furnace (SAF) which is widely used in manganese ferroalloy producing, "freeze" lining is applied in order to insulate the refractory and prevent direct contact with molten metal and slag [13]. "Freeze" lining can enhance the refractory lifetime because it prevents the wear mechanism; such as alkali attack, thermal stress and dissolution of refractory. According to Steenkamp et al. [14], who measured thermal conductivity in the $\text{CaO-SiO}_2\text{-Al}_2\text{O}_3\text{-MgO-MnO}$ system, "freeze" lining becomes thicker with higher thermal conductivity indicating that thermal conductivity is the major factor determining the thickness of "freeze" lining.

The observed thermal conductivity, called effective thermal conductivity (λ_{eff}), can be expressed by the summation of each different thermal conductivity such as lattice thermal conductivity (λ_L), radiation thermal conductivity (λ_R) and electronic thermal conductivity (λ_{el}) [15]

$$\lambda_{eff} = \lambda_L + \lambda_R + \lambda_{el} \quad (1)$$

The lattice thermal conductivity (λ_L) is based on the heat transfer by phonon. Because scattering of phonon results in the decrease in thermal conductivity, thermal conductivity by phonon is significantly influenced by the change of disordering of network structure in the glass and molten oxide system [16]. Over the 800 K, radiative heat transfer (λ_R) in the clear glass becomes dominant factor [17]. At higher temperature of the transparent molten oxide system, more than 90% of heat is transferred by the radiation conduction. On the other hand, thermal conductivity by electron is insignificant in the molten oxide system as long as the composition of transition metallic oxide does not exceed 70% [15, 18].

In the molten oxide system, the radiative heat conduction can be simply predicted by assuming the steady state along with grey-body conditions. The radiative heat transfer through an optically thick sample can be calculated by a function of absorption coefficient and refractive index in the Stefan-Boltzmann law [15]. However, due to its tremendous radiative and convection effect, precise measurement of thermal conductivity by phonon in the molten oxide system was challenging. Recently, owing to the appropriate modifications [2, 4, 19] and evaluations for systematic error by simulation [20], thermal conductivity measurement technique in the molten oxide system has been improved.

In this chapter, transient hot-wire method that is one of the major thermal conductivity measurement techniques for molten oxide system is introduced comparing with laser flash method. The measurement principle is simply dealt with, and experimental errors are considered. In addition, thermal conduction mechanism in the amorphous system by phonon is discussed. Since the lattice thermal conduction is mainly determined by the structure of oxide system, the effect of structure such as silicate network or ionic bonding, and type of cation is briefly discussed.

2. Thermal conduction in glass and molten oxide system

Ziman [21] explained the transport of heat in terms of collective model instead of individual particle vibration. Namely, thermal energy is the distribution of normal modes of vibration. Owing to the collective model, the excitations that can be considered as the movement of particles in a gas, and kinetic theory is possibly adopted. In the case of glass and ceramic system, determination of a single Brillouin zone is impossible since there is no regular lattice. For this reason, not Umklapp scattering but irregular structure determines the phonon scattering in the glass system. Kingery [22] reported that the phonon interaction by discrete lattice is equivalent to random scattering in the ceramic and glass system. For convenience, he adopted mean free path concept and expressed thermal conductivity by phonon as the transport of energy by particle. As a result, thermal conductivity has been simply explained by the phonon gas model in various glass and ceramic systems [16, 23, 24].

$$\lambda = \frac{1}{3} C \bar{v} l \quad (2)$$

where λ , C , \bar{v} and l indicate thermal conductivity, heat capacity, mean particle velocity, and mean free path of collision.

However, the heat transfer mechanism in the liquid and molten oxide system is still controversial. In the liquid state, Zwanzig [25] proposed the collective dynamical variables having the similar characteristic of longitudinal and transverse phonon. The frequency of the elementary excitation is defined as approximate eigenvalue by an eigen function of the Liouville operator. In addition, he also calculated the lifetimes of elementary excitations reporting that it is determined by the elastic moduli and viscosities. As a result, in the molten oxide system which has enough viscosity coefficients, an elementary excitation has physical meaning. Recently, using *ab initio* molecular dynamics simulations, Iwashita et al. [26] showed that the local configurational excitations in the atomic connectivity network are the elementary excitations in molten metal at high temperature.

Turnbull [27] found that thermal conduction mechanism in the molten salts system is similar to the solid state. Due to the similar ionic spacing of salt system in the solid and liquid state along with the relatively small heat of fusion, he assumed that thermal motion would be similar in liquid and solid. In addition, according to his calculation, the diffusional contribution to thermal conductivity of liquids does not exceed 4%, indicating the major role of vibrational conduction in heat transfer. Similar to molten salt system, it can be inferred that heat is mainly transferred by vibrational excitations in the molten oxide system.

Recently, considering the similar thermal conduction mechanism in glass and molten oxide system, Kim and Morita [28] explained the effect of temperature on thermal conductivity following the same approach. Adopting the one-dimensional Debye temperature and phonon gas model, variables and effect of temperature on thermal conductivity were discussed. According to their work, thermal conductivity of glass initially increases with increasing temperature due to the increase of heat capacity. At one-dimensional Debye temperature where heat capacity becomes max, thermal conductivity reaches the maximum. Afterward, owing to the fluidity of molten state, mean particle velocity along with mean free path of collision decreases with increasing temperature. From physical viewpoint, as increasing

temperature, the required frequency of shear waves to propagate in molten oxide system increases. Since phonon is bosonic particle, the average number of particles follows Bose-Einstein distribution indicating that lower frequency modes have more phonons at a fixed temperature. As a result, negative temperature dependence of thermal conductivity can be found because lower number of shear wave with much higher frequency can propagate as temperature increases.

3. Thermal conductivity measurement technique and related experimental errors

3.1. Thermal conductivity measurement technique for high-temperature oxide melts

Although the understanding of thermal conductivity by phonon is significant for the process control in the iron-making and steel-making field, precise measurement of thermal conductivity by phonon is challenging due to the notorious radiation and convection effect at high temperature [29]. The measurement method of thermal conductivity by phonon can be classified into largely two groups: one is steady-state and another one is nonsteady-state method. In steady-state method, thermal conductivity is determined by the temperature profile across a sample contacting directly with a heat source [15]. However, steady-state method requires a relatively long measurement time in order to obtain the steady state of thermal profile across the sample [18]. In addition, during the measurement, contribution of radiation and convection becomes significant due to the long measurement time. For these reasons, at high temperature, thermal conductivity by phonon transfer cannot be precisely measured by using steady-state method.

In order to investigate the thermal conductivity of molten oxide system, nonsteady-state measurement method has been modified for the last few decades. For the measurement of molten oxide system, two measurement techniques have been widely adopted: one is laser flash method and another one is hot-wire method. Two techniques have in common that both two methods apply constant energy and monitor the temperature change with time. Because the thermal conductivity can be measured within approximately 10 s by nonsteady-state method, the effect of radiation and convection is insignificant as compared to the steady-state method.

Since the first introduction of laser flash method in 1961, this technique has been widely adopted for the purpose of measurement of thermal diffusivity and heat capacity in various materials [30]. During the measurement, the front surface is heated by a single pulse laser resulting in an increasing of temperature at the opposite surface. Then, thermal diffusivity is calculated from the increasing temperature. However, due to the leakage of heat from measurement sample, the sufficient accuracy cannot be achieved at high temperature. Several improvements of laser flash method have been introduced in order to overcome various problems occurred during the measurement. In the 1990s, Ogura et al. [31] developed three-layered laser flash method. Although it has the merit of relatively small heat leakage, calculation of thermal conductivity by phonon transfer requires various physical properties related with radiation such as absorption coefficient [32]. For this reason, recently, Ohta et al. [32, 33], revised the three-layered laser flash method and introduced new method,

called front heating-front-detection laser flash method. Distinct from previous laser flash methods, the laser pulse is irradiated on the bottom of platinum crucible during the front-heating front-detection technique. Assuming the one-dimensional heat flow along with semi-infinite thickness of liquid sample, [33] thermal conductivity is calculated by the measurement of the temperature decay at the bottom of surface. Since the thermal conductivity is measured within only 12 ms, front-heating front detection technique does not consider the additional process for distinguishing radiation effect from observed thermal conductivity data. However, although the front heating-front detection laser flash method has the merit of simple procedure and easy data processing, [34] the effect of radiation on thermal conductivity measurement is still controversial, especially at high temperature [18]. The three different laser flash methods, namely, conventional, three-layered and front heating-front detection laser flash method, have been adopted for the measurement of thermal conductivity, and more details can be found elsewhere [18].

Figure 1 shows the schematic diagram of the hot-wire method for molten oxide system. The hot-wire method, also known as line-source method, is a nonsteady-state method. Because the hot-wire method uses a very thin metal wire, the effect of radiation is relatively insignificant even at high temperature [35]. Since transient hot-wire technique firstly introduced in the 1780s, this method has been widely used for the precise measurement of thermal conductivity of solid, liquid and even gas phases [36]. During the thermal conductivity measurement of molten oxide system, a thin Pt-13%Rh wire is placed in the middle of molten oxide sample and heated up by the applied constant current. The generated heat is transferred from hot-wire

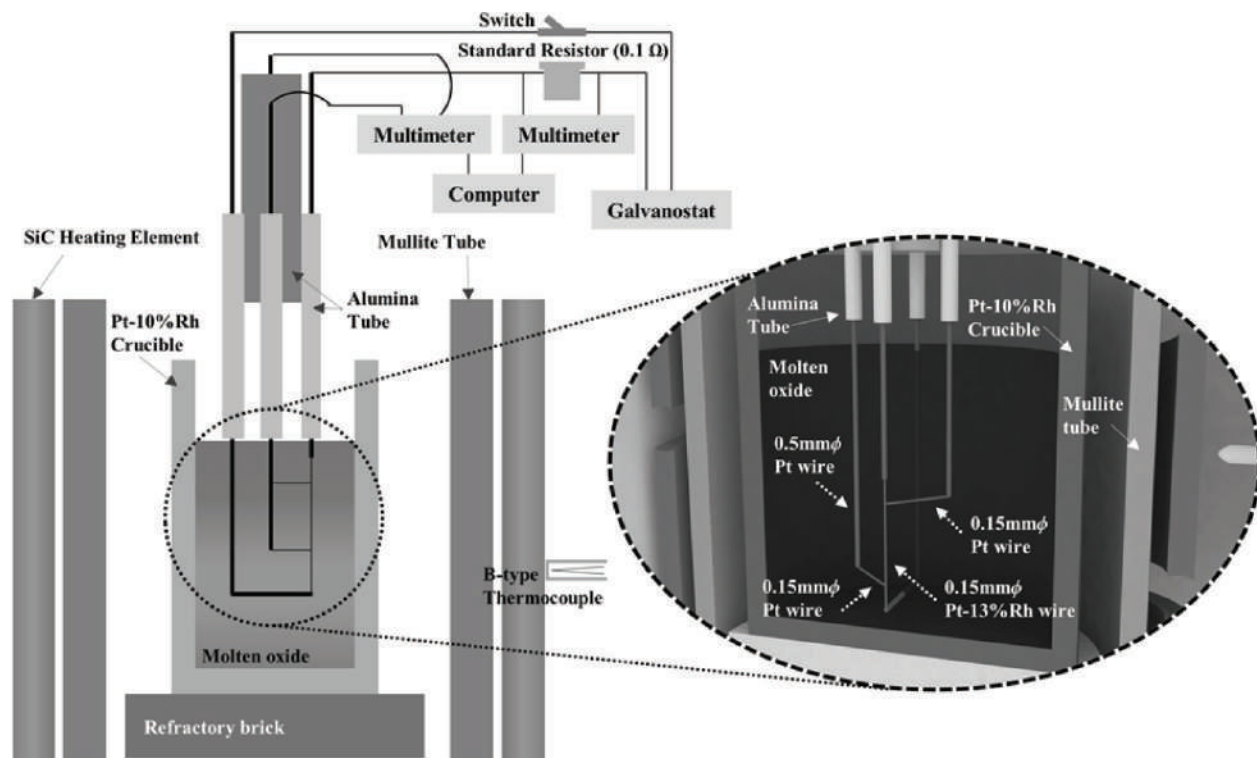


Figure 1. Schematic diagram of the transient hot-wire method for molten oxide system.

into molten oxide system resulting in increasing temperature. If the hot-wire is long enough, the temperature change of molten oxide system resulting from constant heat flux Q can be expressed by a continuous line heat source solution [37].

$$\Delta T = \frac{Q}{4\pi\lambda} \left(\ln \frac{4\kappa t}{r^2} - \gamma \right) = \frac{Q}{4\pi\lambda} \left(\ln t + \ln \frac{4\kappa}{r^2 e^\gamma} \right) \quad (3)$$

Here, ΔT is the temperature change of hot-wire, Q is the heat generation per unit length of hot-wire, λ is the thermal conductivity, κ is the thermal diffusivity, r is the radius of hot-wire, t is the time, and γ is the Euler's constant, 0.5772. The continuous line heat source solution can be adopted when the length and diameter ratio of hot-wire is larger than 30 [38]. Following the differentiation of Eq. (3), thermal conductivity can be expressed by Eq. (4).

$$\lambda = \left(\frac{Q}{4\pi} \right) / \left(\frac{dT}{d \ln t} \right) \quad (4)$$

Because a constant current is applied by galvanostat, heat generations per unit length of hot-wire (Q) can be calculated by the following equation.

$$Q = \frac{VI}{m} = I^2 \frac{R_T}{m} \quad (5)$$

$$R_T = R_0(1 + AT + BT^2) \quad (6)$$

The abovementioned equation, V , I , m , R_T and R_0 represents the voltage, current, length of hot-wire, resistance per unit length at $T^\circ\text{C}$, and resistance per unit length at 0°C , respectively. Eq. (6) shows the empirical linear relationship between R_T and R_0 . According to Kang and Morita [3], constant of A and B for Pt-13%Rh wire is 1.557×10^{-3} and -1.441×10^{-7} , respectively. During the measurement, R_T is obtained by applying infinitely small current which could not heat up the experimental sample.

From the Ohm's law, the following equation can be obtained at the given temperature T .

$$\frac{dV}{dT} = I \frac{dR_T}{dT} = IR_0(A + 2BT) \quad (7)$$

From the Eqs. (4), (5) and (7), the thermal conductivity can be expressed as the function of voltage and time.

$$\lambda = \left(\frac{I^3 R_T R_0 (A + 2BT)}{4m\pi} \right) / \left(\frac{dV}{d \ln t} \right) \quad (8)$$

Using the four-terminal sensing, [11] the voltage change of hot-wire is recorded in real time. Therefore, thermal conductivity of the molten oxide system can be easily calculated by the slope of V versus $\ln t$.

Recently, Mills et al. [39] found that thermal conductivity of molten slag system measured by laser flash method is approximately 10 times than by hot-wire method implying the effect of radiation in the laser flash method. Therefore, it would be inferred that thermal conductivity of molten oxide system is precisely measured at high temperature by using the hot-wire method rather than using the laser flash method.

3.2. Evaluation of the experimental errors occurred during the thermal conductivity measurement by hot-wire method

According to Kwon and Lee [40] and Healy et al. [41] who studied about the errors occurred during the thermal conductivity measurement, appropriately designed hot-wire method can measure thermal conductivity of liquid with the error of less than 0.31%. Although they considered low temperature, below 100°C, effect of other variables such as convection and current leakage seems insignificant during the thermal conductivity measurement even at high temperature.

As previously mentioned, in order to reduce the radiative heat transfer, a thin Pt-13%Rh wire of 0.15 mm ϕ is used in the hot-wire method during the thermal conductivity measurement. However, although a hot-wire method uses extremely thin wire, the heat can be transferred from the surface of hot-wire by radiation and it becomes significant as temperature increases during the thermal conductivity measurement.

Using the Stefan–Boltzmann law for grey-body radiation, the radiation heat at the surface of hot wire was estimated.

$$q = \varepsilon E_b = \varepsilon \sigma T_s^4 \quad (9)$$

where q is the radiated heat energy, ε is the emissivity, σ is the Stefan-Boltzmann constant, T_s is the surface temperature (K). During the calculation, emissivity of Pt-13%Rh wire was extrapolated on the basis of empirical equation of emissivity of Pt- 10%Rh wire [42]

$$\varepsilon = 0.751 (T\rho)^{0.5} - 0.632(T\rho) + 0.670 (T\rho)^{1.5} - 0.607 (T\rho)^2 \quad (10)$$

where ρ is the resistivity, and T is the temperature of hot-wire (°C). The temperature change of hot-wire along with heat generation was evaluated by the voltage change. Considering the resistivity of hot-wire, the radiation heat during the measurement was evaluated. In **Figure 2**, change of radiation heat along with applied power at 1273 K is presented. After 5 s of experiment, the ratio of radiation heat to the applied power, which is the net heat flow, becomes approximately 0.69% at 1273 K. This value is accordance with the previously calculated value of 1% in the transparent slag at 1273 K after 5 s of experiment [2]. Especially, within the thermal conductivity measurement region, which is 0.8–2 s, radiation heat takes less than 0.51% over total heat flow. Therefore, it can be concluded that radiation effect is not significant during the thermal conductivity measurement using a hot-wire method.

The effect of free convection can be reduced by placing the upper level of the sample in the highest temperature zone [4]. However, during the measurement, the heating up of hot-wire

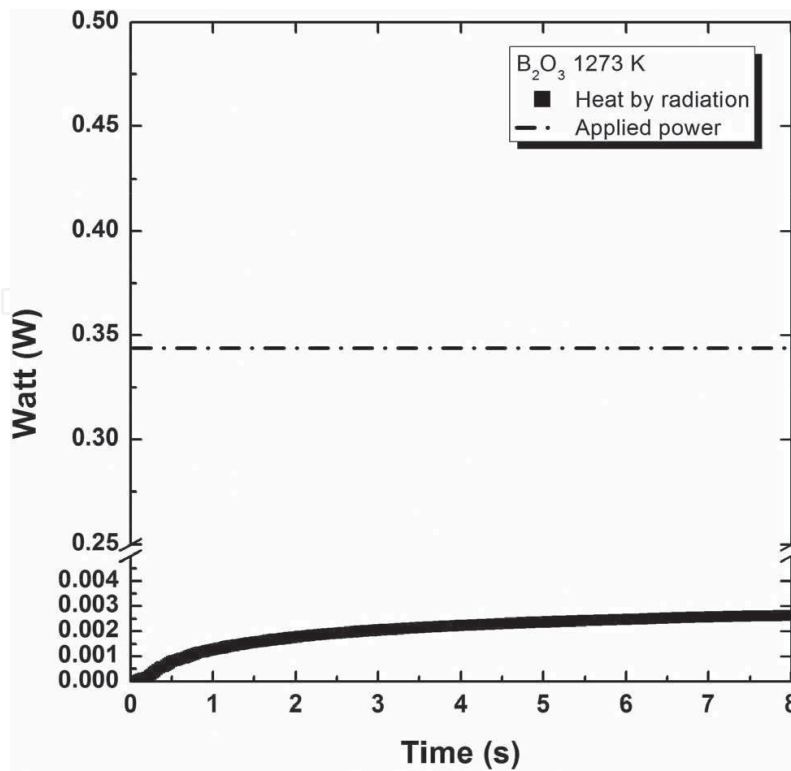


Figure 2. Change of radiation heat (black rectangular) with varying time at a fixed temperature of 1273 K. Dashed dot line indicates the applied power.

results in the increase in temperature of molten oxide system along with partial temperature difference. Such temperature gradient would lead to the convection. In order to determine the effect of convection, the change of Rayleigh number with varying time was considered. **Figure 3** shows the schematic diagram of heat penetration during a hot-wire measurement.

When a current is applied, heat is generated in a thin hot-wire; radius of r_0 . Since it is a non-steady-state method, the heat penetration distance will be varying with time. δ is the penetration distance. T_0 and T_1 is the temperature at the surface of hot-wire and the temperature at δ , respectively. The heat penetration distance (δ) is a function of time (t). Tokura et al. [43] reported that heat penetration distance from the hot-wire can be expressed by the following equation.

$$\delta \approx (24\alpha r_0 t)^{1/3} + r_0 \quad (11)$$

The abovementioned Eq. (11) is valid when $(\delta - r_0) \gg 4r_0$. α represents the thermal diffusivity.

It has been reported that free convection is occurred when Rayleigh number (Ra) is larger than 1000 [1]. Therefore, calculation of Rayleigh number in the present molten oxide system is significant in order to evaluate the effect of free convection during the experiment. Rayleigh number can be expressed by the following equation, which is the product of Grashof number and Prandtl number.

$$Ra = \frac{\beta \Delta T g L^3}{\nu \alpha} \quad (12)$$

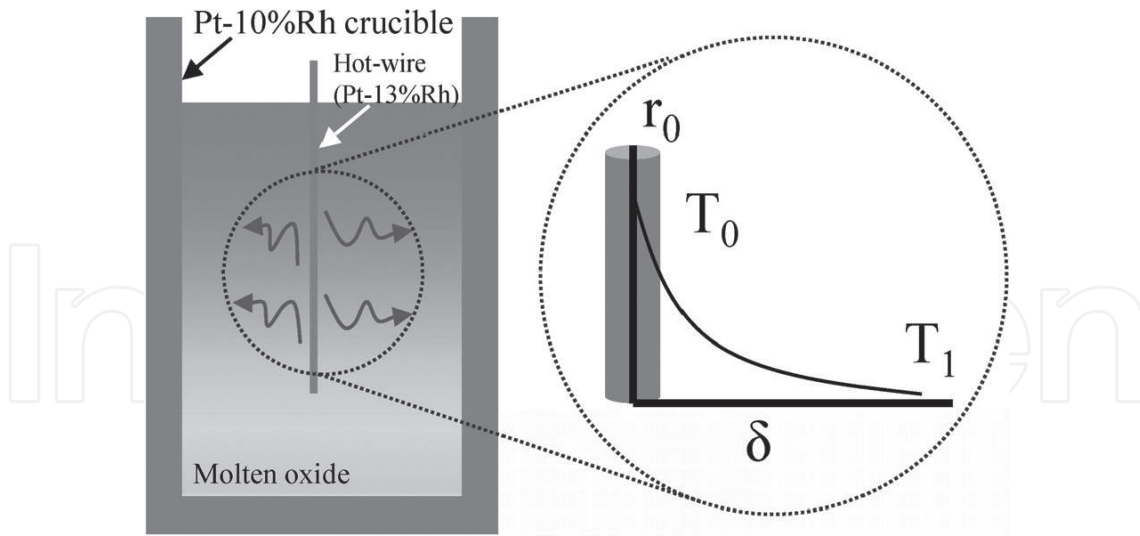


Figure 3. Schematic diagram of heat penetration during thermal conductivity measurement by hot-wire measurement.

where β is thermal expansion coefficient, ΔT is temperature difference, g is gravitational acceleration, L is characteristic length, ν is kinetic viscosity. L can be substituted with heat penetration distance (δ). Combine the Eqs. (3), (11) and (12), Rayleigh number can be deduced by the following equation, where C is the exponential of Euler's constant; 1.78.

$$Ra = \frac{\beta g Q}{4\pi\lambda\nu\alpha} [(24\alpha r_0 t)^{1/3} + r_0]^3 \ln\left(\frac{4\alpha t}{r_0^2 C}\right) \quad (13)$$

Using Eq. (13) along with following physical properties of molten B_2O_3 system at 1273 K, Rayleigh number can be calculated. Thermal expansion coefficient (β) of molten B_2O_3 is 100 ppm/K at the temperature range between 1273 and 1473 K [44]. Thermal diffusivity (α) is $4.325 \text{ cm}^2 \text{ s}^{-1}$ at 1273 K [31]. Kinematic viscosity, that is, the ratio of dynamic viscosity to density is $0.0065 \text{ m}^2 \text{ s}^{-1}$ [45]. Rayleigh number is calculated, and it is shown in **Figure 4**. Compared to Rayleigh number of pure water at 298 K, molten B_2O_3 system shows much lower Rayleigh number. Due to much higher kinematic viscosity and thermal diffusivity, B_2O_3 shows much lower Rayleigh number even at high temperature of 1273 K. Therefore, it can be concluded that there is no free convection effect during the thermal conductivity measurement of molten oxide system within 10 s. In addition, if there is convection effect, the linearity between voltage and time could not be observed. As a result, the thermal conductivity by phonon transfer can be safely obtained within the region where the linear relationship between voltage and time exists.

Recently, several studies have evaluated the experimental conditions which affect precision of the measurement using hot-wire method [20, 46]. A computational fluid dynamics (CFD) calculation [20] revealed that determination of the resistivity and the temperature coefficient of resistance of the hot-wire is crucial in order to obtain precise thermal conductivity. In addition, Kang et al. [46] calculated the current leakage by semi-quantitative evaluation and reported that the current leakage is 2% (at most) in various silicate melts which contain less than 20 wt% FeO_x .

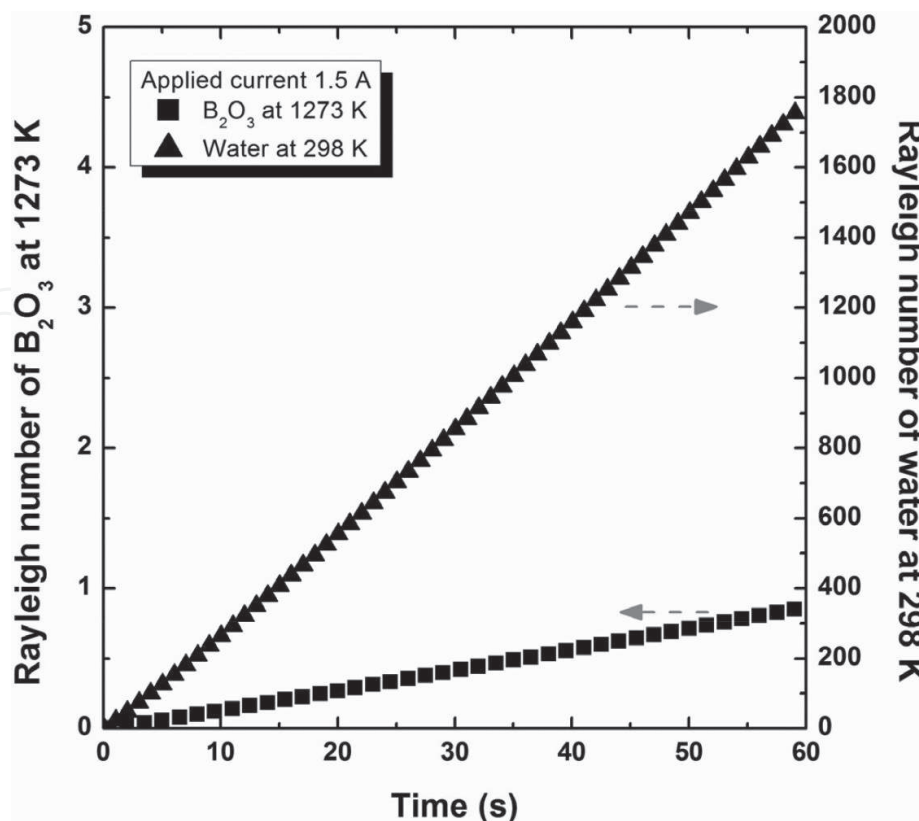


Figure 4. Calculated Rayleigh number of molten B₂O₃ at 1273 K (left) and water at 298 K (right) with varying time.

4. Effect of structure and cation on thermal conductivity of molten oxide system

Similar to other physical properties, such as density, thermal expansion, viscosity and electric conductivity, thermal conductivity of molten oxide system is affected by the network structure such as silicate, borate and aluminate network structures. It was known that formation of network structure in the glass and molten oxide system plays a role of limiting to the network randomness [47] resulting in the increase of thermal conductivity by reducing of phonon-phonon scattering. According to Kang and Morita [3], depolymerization of silicate network structure results in lowering thermal conductivity. In addition, amphoteric behavior of aluminum oxide related to aluminate structure leads to both increasing and decreasing of thermal conductivity depending on its compositions. Recently, Kim and Morita reported the effect of intermediate range order borate structure [48–52]. In case of borate structure, complicated super-structure units exist consisting of 3- and 4-coordinate boron ions associated with oxygen ions [53]. Depending on the compositions and oxide system, different borate super-structure can be formed resulting in different effects on thermal conductivity.

In Figure 5, thermal conductivity of molten Na₂O-B₂O₃-SiO₂ system is shown with varying SiO₂/B₂O₃ mole ratio [49]. At 1273 K, increasing of thermal conductivity with higher ratio of SiO₂/B₂O₃ can be found. Although these systems show similar silicate network structures with

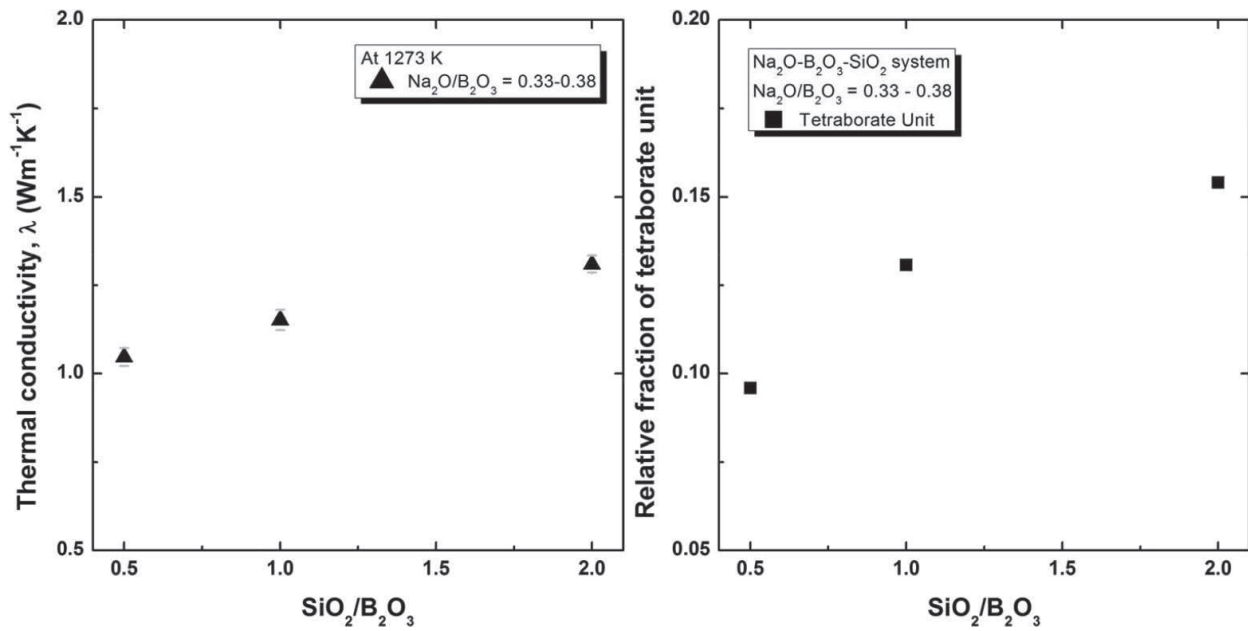


Figure 5. Relationship between $\text{SiO}_2/\text{B}_2\text{O}_3$ ratio and the thermal conductivity (left), $\text{SiO}_2/\text{B}_2\text{O}_3$ ratio and relative fraction of tetraborate unit (right).

analogous non-bridging oxygen (NBO) number [49]. On the right side of **Figure 5**, the effect of $\text{SiO}_2/\text{B}_2\text{O}_3$ ratio on borate super-structure obtained by Raman spectroscopy is shown. It should be noted that the Raman spectra were identified by using Gaussian deconvolution from appropriate references. According to area ratio, the relative fraction of associated structures was calculated. The increase of relative fraction of tetraborate unit can be found with higher concentration of SiO_2 . Considering that tetraborate unit consisting of 3- and 4-coordinate boron forms three-dimensional network, thermal conductivity increases as a result of polymerization of the network structure. Similar effect can be found in another study reporting the increase of viscosity with formation of tetraborate unit in the $\text{CaO}-\text{Al}_2\text{O}_3-\text{Na}_2\text{O}-\text{B}_2\text{O}_3$ system [54].

Not only the polymerized network structure, but also cation affects thermal conductivity in the molten oxide system [8, 28, 51, 55]. The linear relationship between thermal conductivity and ionization potential (Z/r^2); the ratio of the charge of the cation (Z) to the square of the cation radius (r), was observed in the alkali-borate system [28, 51]. In addition, the effect of ionization potential of cation on thermal conductivity is similar in both glass and molten oxide system. Recently, Crupi et al. [56] reported that intermediate range order borate structure, that is borate super-structure, is affected by the type of cations. As increasing of the ionic radius of cation, larger radius of void can be found. Since larger void has high flexibility with high configurations, thermal conductivity decreases as increasing of ionic radius [28].

5. Conclusions

In this chapter, the thermal conductivity measurement technique for high-temperature molten oxide system was reviewed along with heat conduction. Although phonon cannot be

defined in the molten oxide system, phonon-like excitation is elementary excitation having similar characteristic of longitudinal and transverse phonon. Recent studies revealed that local configurational excitation is a origin of phonon-like excitation. In addition, the effect of temperature on thermal conductivity in both glass and molten oxide system was reviewed. The laser flash method and hot-wire method, typical thermal conductivity measurement techniques for high temperature, were briefly reviewed. Compared to laser flash method, hot-wire method is relatively precise for measurement of molten oxide system by reducing radiation effect through small surface of heating source. The systematic errors probably occurred were considered. The radiation and convection effects were reviewed based on the simple modeling and mathematical calculations in the molten oxide system. Results showed that radiation effect and convection effect on thermal conductivity are insignificant at 1273 K. Especially, since the measurement is terminated within 5 s, its effect would be negligible. Finally, the effect of network structure and cations on thermal conductivity was discussed. Due to limiting its randomness, polymerization of glass and molten oxide system results in the increase of thermal conductivity. In addition, the effect of cation type on thermal conductivity in the molten oxide system was discussed through the ionization potential.

Acknowledgements

Youngjae Kim is grateful for the financial support that was provided by the Basic Research Project (GP2017-025) of the Korea Institute of Geoscience and Mineral Resources (KIGAM), funded by the Ministry of Science and ICT.

Author details

Youngjae Kim^{1*}, Youngjo Kang² and Kazuki Morita³

*Address all correspondence to: youngjae.kim@kigam.re.kr

1 Korea Institute of Geoscience and Mineral Resources, Republic of Korea

2 Dong-A University, Republic of Korea

3 The University of Tokyo, Japan

References

- [1] Kang Y. Thermal Conductivity of $\text{Na}_2\text{O-SiO}_2$ and $\text{CaO-Al}_2\text{O}_3\text{-SiO}_2$ melt [thesis]. The University of Tokyo; 2004
- [2] Nagata K, Goto KS. Heat conductivity and mean free path of phonons in metallurgical slags. In: Fine HA, Gaskell DR, editors. Second International Symposium on

- Metallurgical Slags and Fluxes. Warrendale: The Metallurgical Society of AIME; 1984. pp. 875-889
- [3] Kang Y, Morita K. Thermal conductivity of the CaO-Al₂O₃-SiO₂ system. *ISIJ International*. 2006;**46**(3):420-426
- [4] Nagata K, Susa M, Goto KS. Thermal conductivities of slags for ironmaking and steel-making. *Tetsu-to-Hagane*. 1983;**11**(11):1417-1424
- [5] Hasegawa H, Hoshino Y, Kasamoto T, et al. Thermal conductivity measurements of some synthetic Al₂O₃-CaO-SiO₂ slags by means of a front-heating and front-detection laser-flash method. *Metallurgical and Materials Transactions B*. 2012;**43**(6):1405-1412. DOI: 10.1007/s11663-012-9702-y
- [6] Glaser B, Sichen D. Thermal conductivity measurements of ladle slag using transient hot wire method. *Metallurgical and Materials Transactions B*. 2012;**44B**(1):1-4. DOI: 10.1007/s11663-012-9773-9
- [7] Kang Y, Nomura K, Tokumitsu K, Tobo H, Morita K. Thermal conductivity of the molten CaO-SiO₂-FeO_x system. *Metallurgical and Materials Transactions B*. 2012;**43**(6):1420-1426. DOI: 10.1007/s11663-012-9706-7
- [8] Ozawa S, Susa M. Effect of Na₂O additions on thermal conductivities of CaO-SiO₂ slags. *Ironmaking & Steelmaking*. 2005;**32**(6):487-493
- [9] Qiu X, Xie B, Qing X, Diao J, Huang Q, Wang S. Effects of transition metal oxides on thermal conductivity of mould fluxes. *Journal of Iron and Steel Research, International*. 2013;**20**(11):27-32. DOI: 10.1016/S1006-706X(13)60192-2
- [10] Susa M, Kubota S, Hayashi M, Mills KC. Thermal conductivity and structure of alkali silicate melts containing fluorides. *Ironmaking & Steelmaking*. 2001;**28**(5):390-395. DOI: 10.1179/irs.2001.28.5.390
- [11] Ozawa S, Endo R, Susa M. Thermal conductivity measurements and prediction for R₂O-CaO-SiO₂ (R= Li, Na, K) slags. *Tetsu-to-Hagane*. 2007;**93**(6):416-423
- [12] Mills KC. The influence of structure on the physico-chemical properties of slags. *ISIJ International*. 1993;**33**(1):148-155. DOI: 10.2355/isijinternational.33.148
- [13] Duncanson PL, Toth JD. The truths and myths of freeze lining technology for submerged arc furnaces. In *INFACON X: Transformation Through Technology*, The South African Institute of Mining and Metallurgy: Cape Town, South Africa, 2004; 488-499
- [14] Steenkamp JD, Tangstad M, Pistorius PC. Thermal conductivity of solidified manganese-bearing slags—a preliminary investigation. In: Jones RT, den Hoed P, editors. *Southern African Pyrometallurgy 2011 International Conference*. Johannesburg: The Southern African Institute of Mining and Metallurgy; 2011. pp. 327-344
- [15] Mills KC. *Slag Atlas*, Verein Deutscher Eisenhüttenleute (VDEh). 2nd ed. Dusseldorf: Verlag Stahleisen GmbH; 1995
- [16] Kittel C. Interpretation of the thermal conductivity of glasses. *Physical Review*. 1949; **75**(6):972-974

- [17] De Jong BHWS, Beerkens RGC, van Nijnatten PA, Le Bourhis E. Glass, 1. Fundamentals. In: Ullmann's Encyclopedia of Industrial Chemistry. Weinheim: Wiley-VCH; 2000. DOI: 10.1002/14356007
- [18] Kang Y, Lee J, Morita K. Thermal conductivity of molten slags: A review of measurement techniques and discussion based on microstructural analysis. ISIJ International. 2014;**54**(9):2008-2016. DOI: 10.2355/isijinternational.54.2008
- [19] Ogino K, Nishiwaki J, Yamamoto Y. Suragu yuutai no netsudendoudo no sokutei [Thermal conductivity measurement in the molten slag]. Tetsu- to- Hagane. 1979;**65**(11):S683
- [20] Glaser B, Ma L, Sichen D. Determination of experimental conditions for applying hot wire method to thermal conductivity of slag. Steel Research International. 2013;**84**(7):649-663. DOI: 10.1002/srin.201200206
- [21] Ziman JM. Electrons and Phonons: The Theory of Transport Phenomena in Solids. London: Oxford University Press; 1960
- [22] Kingery WD. Introduction to Ceramics. New York: Wiley; 1967
- [23] Tohmori M, Sugawara T, Yoshida S, Matsuoka J. Thermal conductivity of sodium borate glasses at low temperature. Physics and Chemistry of Glasses - European Journal of Glass Science and Technology Part B. 2009;**50**(6):358-360
- [24] Zeller RC, Pohl RO. Thermal conductivity and specific heat of noncrystalline solids. Physical Review B. 1971;**4**(6):2029-2041
- [25] Zwanzig R. Elementary excitations in classical liquids. Physical Review. 1967;**156**(1):190-195. DOI: 10.1103/PhysRev.156.190
- [26] Iwashita T, Nicholson DM, Egami T. Elementary excitations and crossover phenomenon in liquids. Physical Review Letters. 2013;**110**(20):205504. DOI: 10.1103/PhysRevLett.110.205504
- [27] Turnbull AG. The thermal conductivity of molten salts II. Theory and results for pure salts. Australian Journal of Applied Science. 1961;**12**:324-329
- [28] Kim Y, Morita K. Temperature dependence and cation effects in the thermal conductivity of glassy and molten alkali borates. Journal of Non-Crystalline Solids. 2017;**471**:187-194. DOI: 10.1016/j.jnoncrysol.2017.05.034
- [29] Nagashima A. Viscosity, thermal conductivity, and surface tension of high-temperature melts. International Journal of Thermophysics. 1990;**11**(2):417-432. DOI: 10.1007/BF01133571
- [30] Waseda Y, Ohta H. Current views on thermal conductivity and diffusivity measurements of oxide melts at high temperature. Solid State Ionics. 1987;**22**:263-284
- [31] Ogura G, Suh I-K, Ohta H, Waseda Y. Thermal diffusivity measurement of boron oxide melts by laser flash method. Journal of the Ceramic Society of Japan. 1990;**98**(3):305-307
- [32] Ohta H, Shibata H, Waseda Y. Recent progress in thermal diffusivity measurement of molten oxides by the laser flash method. In: Kongoli F, Itagaki K, Yamauchi C, Sohn HY,

- editors. Yazawa International Symposium. San Diego: TMS (The Minerals, Metals & Materials Society); 2003. pp. 453-462
- [33] Ohta H, Shibata H, Hasegawa H, et al. Thermal conductivity of R-Na₂O-SiO₂ (R = Al₂O₃, CaO) melts. *Journal for Manufacturing Science & Production*. 2013;**13**(1-2):115-119. DOI: 10.1515/jmsp-2012-0020
- [34] Hasegawa H, Ohta H, Shibata H, Waseda Y. Recent development in the investigation on thermal conductivity of silicate melts. *High Temperature Materials and Processes*. 2012;**31**(4-5):491-499. DOI: 10.1515/htmp-2012-0085
- [35] Mills KC, Yuan L, Li Z, Zhang G. Estimating viscosities, electrical & thermal conductivities of slags. *High Temperatures – High Pressures*. 2013;**42**:237-256
- [36] Assael MJ, Antoniadis KD, Wakeham WA. Historical evolution of the transient hot-wire technique. *International Journal of Thermophysics*. 2010;**31**(6):1051-1072. DOI: 10.1007/s10765-010-0814-9
- [37] Carslaw HS, Jaeger JC. *Conduction of Heat in Solids*. 2nd ed. London: Oxford University Press; 1959
- [38] Blackwell J. The axial-flow error in the thermal-conductivity probe. *Canadian Journal of Physics*. 1956;**34**(4):412-417
- [39] Mills KC, Yuan L, Jones RT. Estimating the physical properties of slags. *Journal of the Southern African Institute of Mining and Metallurgy*. 2011;**111**(10):649-658
- [40] Kwon SY, Lee S. Precise measurement of thermal conductivity of liquid over a wide temperature range using a transient hot-wire technique by uncertainty analysis. *Thermochimica Acta*. 2012;**542**:18-23. DOI: 10.1016/j.tca.2011.12.015
- [41] Healy JJ, de Groot JJ, Kestin J. The theory of the transient hot-wire method for measuring thermal conductivity. *Physica B+C*. 1976;**82**(2):392-408. DOI: 10.1016/0378-4363(76)90203-5
- [42] Bradley D, Entwistle AG. Determination of the emissivity, for total radiation, of small diameter platinum-10% rhodium wires in the temperature range 600-1450 C. *British Journal of Applied Physics*. 1961;**12**(12):708-711. DOI: 10.1088/0508-3443/12/12/328
- [43] Tokura I, Saito H, Kishinami K, Takekawa Y. Application of the transient hot-wire method on thermal conductivity measurement of solid-liquid mixtures. *Memoirs of the Muroran Institute of Technology. Science and Engineering*. 1990;**40**:63-73
- [44] Shartsis L, Capps W, Spinner S. Density and expansivity of alkali borates and density characteristics of some other binary glasses. *Journal of the American Ceramic Society*. 1953;**36**(2):35-43. DOI: 10.1111/j.1151-2916.1953.tb12833.x
- [45] Napolitano A, Macedo PB, Hawkins EG. Viscosity and density of boron trioxide. *Journal of the American Ceramic Society*. 1965;**48**(12):613-616. DOI: 10.1111/j.1151-2916.1965.tb14690.x

- [46] Kang Y, Lee J, Morita K. Comment on “thermal conductivity measurements of some synthetic Al_2O_3 -CaO-SiO₂ slags by means of a front-heating and front-detection laser-flash method”. *Metallurgical and Materials Transactions B*. 2013;**44**(6):1321-1323. DOI: 10.1007/s11663-013-9933-6
- [47] Kingery WD. Thermal conductivity: XIV, conductivity of multicomponent systems. *Journal of the American Ceramic Society*. 1959;**42**(12):617-627
- [48] Kim Y, Morita K. Relationship between molten oxide structure and thermal conductivity in the CaO-SiO₂-B₂O₃ system. *ISIJ International*. 2014;**54**(9):2077-2083. DOI: 10.2355/isijinternational.54.2077
- [49] Kim Y, Yanaba Y, Morita K. The effect of borate and silicate structure on thermal conductivity in the molten Na₂O-B₂O₃-SiO₂ system. *Journal of Non-Crystalline Solids*. 2015;**415**:1-8. DOI: 10.1016/j.jnoncrsol.2015.02.008
- [50] Kim Y, Morita K. Thermal conductivity of molten B₂O₃, B₂O₃-SiO₂, Na₂O-B₂O₃, and Na₂O-SiO₂ systems. *Journal of the American Ceramic Society*. 2015;**98**(5):1588-1595. DOI: 10.1111/jace.13490
- [51] Kim Y, Morita K. Thermal conductivity of molten Li₂O-B₂O₃ and K₂O-B₂O₃ systems. Smith D (ed). *Journal of the American Ceramic Society*. 2015;**98**(12):3996-4002. DOI: 10.1111/jace.13820
- [52] Kim Y, Yanaba Y, Morita K. Influence of structure and temperature on the thermal conductivity of molten CaO-B₂O₃. *Journal of the American Ceramic Society*. 2017;**100**(12):5746-5754. DOI: 10.1111/jace.15123
- [53] Wright AC. Borate structures: crystalline and vitreous. *Physics and Chemistry of Glasses – European Journal of Glass Science and Technology Part B*. 2010;**51**(1):1-39
- [54] Kim GH, Sohn I. Role of B₂O₃ on the viscosity and structure in the CaO-Al₂O₃-Na₂O-based system. *Metallurgical and Materials Transactions B*. 2013;**45**:86-95. DOI: 10.1007/s11663-013-9953-2
- [55] Hayashi M, Ishii H, Susa M, Fukuyama H, Nagata K. Effect of ionicity of nonbridging oxygen ions on thermal conductivity of molten alkali silicates. *Physics and Chemistry of Glasses*. 2001;**42**(1):6-11
- [56] Crupi C, Carini G, González M, D’Angelo G. Origin of the first sharp diffraction peak in glasses. *Physical Review B*. 2015;**92**(13):134206. DOI: 10.1103/PhysRevB.92.134206